

# Acoustic Measurements of Ice Thickness

Team Members: Liam Cahill

Tristan Kazo

Shan Li

Faculty Advisor: Thomas Weber Ph.D.

## ABSTRACT

The world's climate is dynamic, and one of the most observable aspects of this is the extent and thickness of sea ice. Monitoring the thickness of the ice caps has important scientific, commercial and military applications, yet there are currently few methods to do so precisely and with a high data density. Current practices involve taking direct ice cores, profiling the underside of the ice via aircraft mounted inductance probes or subsurface sonars and combining this data with surface height data obtained by laser altimeters. The focus of this project is to derive a method to determine the thickness of ice to the centimeter level using high resolution, broadband echo sounding techniques from below the ice. In the project's scope, an insulated water tank and cooling system capable of growing ice under constant conditions was designed and constructed. A broadband echosounder was mounted in an upwards facing orientation in the bottom of this tank, along with profiling instrumentation for both temperature and ice thickness. Profile, physical ice core and acoustic data were analyzed and compared to provide correlative measurements. As ice grew, acoustic data was continuously collected, and the observed water-ice and ice-air interfaces were analyzed to determine the thickness of the ice at high resolution. Construction of the 600 gallon closed system tank rendered a final product which could cool and form ice at a rate of  $0.45 \pm 0.08$  cm/day. It was found through a combination of ice core extrapolation and acoustic time series analysis that the acoustic system had an ice thickness resolution of 1.2 cm.

# Table of Contents

<b>List of Figures</b>	5
<b>1. Introduction</b>	6
1.1. Experimental Introduction	6
1.2. Societal Impact	7
<b>2. Acoustic Theory and Predictions</b>	9
2.1. Near-Field, Far-field and Beam Pattern Calculations	9
2.2. Initial Acoustic Pulse Model	11
2.3. Modeling Boundary Interactions/Ice Thickness	12
2.4. Received Pulse Prediction	14
<b>3. Design Considerations</b>	16
3.1. Required Instrumentation	16
3.1.1. Thermistor Array Construction and Calibration	16
3.2. Initial Sizing, Insulation and Cooling Needs	21
3.2.1. Acoustic Near-Field Considerations	21
3.2.2. Heat Transfer Overview	21
3.2.3. Insulation Considerations	22
3.2.4. Cooling System Requirements	23
<b>4. Designs and Modifications</b>	24
4.1. Version 1	25
4.1.1. Design Description	25
4.1.2. Design Flaws	25
4.2. Version 2	26
4.2.1. Design Description	26
4.2.2. Trial Results	28
4.2.3. Design Flaws	28
4.2.4. Design Revisit	29
4.3. Version 3	29
4.3.1. Design Description	29
4.3.2. Trial 2 Results	31
4.3.3. System Analysis	32
<b>5. Acoustic Analysis</b>	35
<b>6. Conclusions</b>	37
<b>7. Future Recommendations</b>	38
<b>8. References</b>	40
<b>Acknowledgements</b>	42
<b>9. Appendices</b>	43
9.1. Arduino Code for Thermistor Array	43

<b>9.2.</b>	<b>MATLAB Code for Temperature Profile</b>	
	47	
<b>9.3.</b>	<b>MATLAB Code for Far-Field and Beam Pattern Model</b>	<b>49</b>
<b>9.4.</b>	<b>MATLAB Code for the Initial and Reflected Pulse Response</b>	<b>51</b>
<b>9.5.</b>	<b>MATLAB Code for Cooling Capacity of the System</b>	<b>54</b>

## List of Figures

<b>Figure 1</b> - Arctic Shipping Lane Diagram	7
<b>Figure 2</b> - Icebreaker Nuclear Submarine Picture	8
<b>Figure 3</b> - Near-Field, Far-Field Graph	9
<b>Figure 4</b> - Beam Pattern Graph	10
<b>Figure 5</b> - Model of Initial Acoustic Pulse Graph	11
<b>Figure 6</b> - Frequency Distribution of Modeled Pulse Graph	12
<b>Figure 7</b> - Reflection and Transmission Diagram	12
<b>Figure 8</b> - Predicted Received Acoustic Response (6.8cm of Ice) Graph	15
<b>Figure 9</b> - ES200-7CD Transducer Picture	16
<b>Figure 10</b> - CAD Model of Thermistor Housing Diagram	17
<b>Figure 11</b> - Thermistor and Arduino Circuit Diagram	18
<b>Figure 12</b> - Thermistor Calibration Overlay Plot	19
<b>Figure 13</b> - One Way Analysis of Thermistor Measurement Difference Graph	19
<b>Figure 14</b> - Waterproofing Thermistor Temperature Response Graph	20
<b>Figure 15</b> - Error in Thermistor Measurements Graph	20
<b>Figure 16</b> - Freezer System Diagram	23
<b>Figure 17</b> - Tank Design Version 2 Diagram	26
<b>Figure 18</b> - Version 2: Tank with Insulation Picture	27
<b>Figure 19</b> - Version 2: Chest Freezer Top with Ventilation Pipes Picture	27
<b>Figure 20</b> - Version 2: Completely Constructed System Picture	27
<b>Figure 21</b> - Version 2: Thermistor Temperature Profile Graph	28
<b>Figure 22</b> - Version 3: Final Tank Design Diagram	29
<b>Figure 23</b> - Version 3: Tank with Insulated Base and Wooden Frame Picture	30
<b>Figure 24</b> - Version 3: Assembly of Outer Wall Insulation Picture	30
<b>Figure 25</b> - Version 3: Salvaged Cooling System Components Picture	30
<b>Figure 26</b> - Version 3: Cooling System Integrated on Tank Lid Picture	30
<b>Figure 27</b> - Version 3: Installed Instrumentation Within the Tank Picture	31
<b>Figure 28</b> - Version 3: Final Tank Design Experimental Setup Picture	31
<b>Figure 29</b> - Version 3: Thermistor Temperature Profile Graph	32
<b>Figure 30</b> - Version 3: Temperature Profile Graph w/Ice Thickness Callout	33
<b>Figure 31</b> - Ice Core Data/Ice Growth Rate Graph	34
<b>Figure 32</b> - Received Acoustic Boundary Layer Response Graph	35
<b>Figure 33</b> - Comparison of Predicted vs. Actual Received Acoustic Signal Grapp	36

# 1. Introduction

## 1.1 Experimental Introduction

The extent and thickness of arctic sea ice is a subject of interest to government, commercial and civilian sectors. Both submarines and surface icebreakers need to know the thickness of this ice in order to find a safe passage or breakthrough point. Scientists also use measurements of ice for multiple purposes from observing climate change. Currently there are three main methods which determine the thickness of sea ice, the first and most accurate being a direct ice core. This involves physically being at the specified site, and taking a sample of the ice to manually measure. This is extremely accurate, but can be dangerous, expensive, and time consuming and only gives a single point measurement.

A second method involves profiling the underside of the ice using sonar obtained via a static system or by submarine. This profile is then compared to known depth of the sonar to determine the draft of the ice. The known draft is combined with freeboard heights of the ice obtained through satellites or laser altimetry to determine the overall ice thickness. This method is accurate to within roughly 0.5 meters, yet it involves a combination of measurements to accurately determine the thickness. Laser altimetry can only make measurements in clear conditions and both types of satellite measurements can only be used during the winter when there is no surface melting of the ice, which significantly changes the characteristics of the response([www.metoffice.gov.uk](http://www.metoffice.gov.uk)).

Finally, measurements can be made from aircraft mounted inductance probes and altimeters. These probes can detect the water ice interface based on variation in inductance and coupled with altimeter measurements of the surface of the ice can in turn provide ice thickness measurements. The combination of inductance and altimeters yields very accurate results, but the need to be carried by aircraft limits range, operating conditions and can be costly ([www.metoffice.gov.uk](http://www.metoffice.gov.uk))

The focus of this project is to derive a method to determine the thickness of ice to the centimeter level using high resolution, broadband echo sounding techniques from below the ice. Using a modeled response of the acoustic wave reflection off of the water-ice and ice-air boundaries the distance between these boundaries, and thus the thickness of the ice, could be determined. The goals of this project were twofold; First, to construct a large insulated water tank capable of constantly growing ice under controlled conditions. Second, to mount an acoustic transducer in an upwards facing orientation in the bottom of the tank, and collect the acoustic reflection data as ice was grown in the tank. This data would then be compared to ice thickness measurements obtained via timelapse footage and physical ice cores to determine the accuracy of the developed theoretical model.

## 1.2 Societal Impact

It is a widely accepted fact by most scientists and people that the average global temperature of the earth is increasing and that this global warming is leading to the decrease of glaciers and icebergs in the northernmost and southernmost latitudes. This melting of the vast sea ice which covers our poles has adverse effects on local wildlife as well as the world's climate as a whole. Polar ice caps reflect a significant amount of sunlight away from the earth's surface thereby preventing the ocean from absorbing that heat from the sun. As the extent of this ice decreases, more sunlight is directed into the ocean surface and the global ocean temperatures begin to rise. This can cause changes to the ocean's circulation, leading to global climate change and rises in sea level (NOAA, 2011).

As temperatures increase heat waves and droughts worsen, evaporation increases and storms intensify due to the additional moisture in the atmosphere. Intensifying weather conditions affect societies in all locations around the world however, along with sea level rise coastal areas could be the the first to be greatly effected. With approximately 40% of the human population living within 100 km (62 mi) of the coast, sea level rise and intensifying weather events can be especially destructive to many coastal societies worldwide (CIESN). The melting of the icecaps and warming of the oceans also forces a wide array of marine and land animals to either adapt or face extinction.

With 90% of the entire world's trade carried by sea, it is obvious that sea level increase would have an impact. On top of this, the shipping lanes in the northern latitudes that travel through/around the northern polar ice cap will be greatly affected by the melting of the polar ice.

Routes will get shortened, however the increase in icebergs due to the melting and breaking apart of the ice caps will introduce another big issue for the shipping routes. Being able to measure the thickness of the ice at different areas will allow for a more comprehensive way to map the shipping lanes out and ensure safety.

The military sector would also benefit from being able to measure the thickness of the ice with one onboard system. A crucial advantage for the military is the mobility of its forces. Specifically for subsurface ice breaking vessels it is important to have an accurate measure and understanding of the ice thickness they are breaching through. Icebreaker nuclear submarines in the arctic could implement this acoustic measurement system on board below the ice to determine ice thickness above the sub before deciding to surface.



**Figure 1:** A diagram showing the different shipping lanes through and around the Arctic. ([https://e360.yale.edu/features/cargo\\_shipping\\_in\\_the\\_arctic\\_declining\\_sea\\_ice](https://e360.yale.edu/features/cargo_shipping_in_the_arctic_declining_sea_ice))



**Figure 2:** An icebreaking nuclear submarine breaching the arctic sea ice

(<https://www.economist.com/science-and-technology/2017/04/12/the-quickest-way-to-break-the-ice-is-by-submarine>)

Since this system would be integrated on the vessel and have a high resolution the submarine would be able to safely surface through the arctic sea ice independently, through their own calculations and measurements.

It is important as a society moving forward to better understand what is occurring to our planet's climate and ice caps, as well as the the rate at which it is occurring. To do this scientists must apply accurate scientific method to obtain data based on this sea ice melt and global temperature to gain a better understanding of the problem. Gaining accurate data and

enough data at a high enough density of the world's total sea ice thickness is not trivial. The refinement and implementation of the processes being tested throughout this experiment using acoustic transducers or arrays to determine the thickness of the ice from below, independent of other measurements or methods could vastly improve both the accuracy and amount of ice thickness data obtained.



## 2. Acoustic Theory and Predictions

### 2.1 Near-Field, Far-Field and Beam Pattern Calculations

To ensure the transducer was the correct distance away from the growing ice it would be measuring the Near-Field/Far-Field prediction of the Simrad ES200-7CD transducer needed to be calculated. The Near-Field/Far-Field model used in this experiment assumed the transducer was an axial piston transducer. To create this model two equations were used. The first, **Eqn. 1** (Kinsler, 1999: Eq.7.4.5) was the equation of the on axis pressure amplitude for an axial piston transducer, as a function of range.

$$P(r) = 2\rho_o c U_o \left| \sin \left\{ \frac{1}{2}kr \left[ \sqrt{1 + (a/r)^2} - 1 \right] \right\} \right| \quad \text{Eqn. 1}$$

Where  $\rho_o$  is the density of the medium,  $c$  is the sound speed through the medium,  $U_o$  is the uniform normal source velocity of the transducer,  $k = \frac{2\pi f}{c}$  is the wave number ( $f$  is the frequency the transducer is vibrating at),  $r$  the range away from the transducer and  $a$  the effective radius of the transducer. For this model with the transducer operating in freshwater at around  $0^\circ C$ ;  $\rho_o = 1000 \text{ kg/m}^3$ ,  $c = 1403 \text{ m/s}$ ,  $U_o = 1 \text{ m/s}$ ,  $f = 200 \text{ kHz}$ ,  $k = 895.68 \text{ radians/m}$ , and  $a = 0.0295 \text{ m}$ . The range term  $r$ , was an array of ranges from 0 m to 1 m created to plot and determine the range at which the Far-Field began.

The second, **Eqn. 2** (Kinsler, 1999: Eq.7.4.7) was the equation for the asymptotic form of the on axis pressure amplitude for an axial piston transducer.

$$P_{ax}(r) = \frac{1}{2}\rho_o c U_o (a/r)ka \quad \text{Eqn. 2}$$

This asymptotic form of the equation was derived from **Eqn. 1** above, solved under the assumptions that  $r/a \gg 1$  and  $r/a > ka/2$  (Kinsler 1999), which holds true for the values used for this transducer ( $r/a = 15.8$  and  $ka/2 = 13.2$ ). This asymptotic form reveals the expected spherical spreading at large enough distances (the Far-Field), and at even larger distances the wave front can be considered and modeled as a plane wave as the radius of curvature becomes large (Kinsler 1999).

In **Figure 3** above the blue line shows the on axis axial piston pressure amplitude with the complicated interference pattern occurring before about

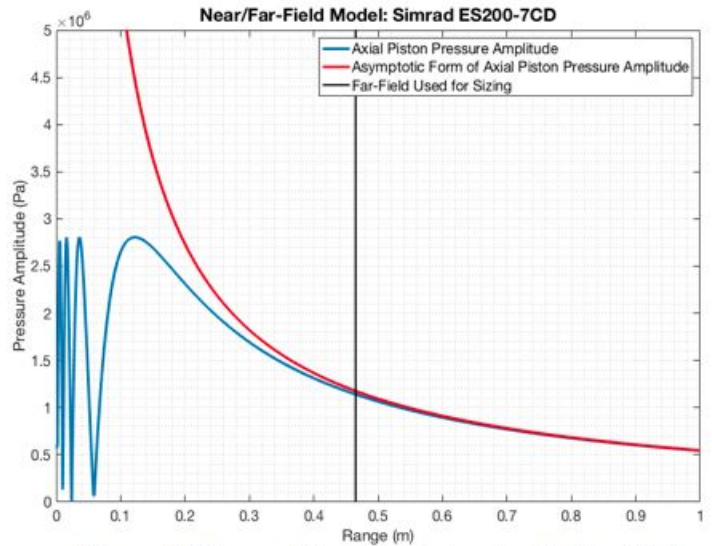


**Figure 3:** The model used to determine the Far-Field distance for the ES200-7CD transducer.

0.2 m (within the Near-Field), and the red line shows the asymptotic solution. The Far-Field distance of approximately 0.45 m was calculated to occur when the on axis axial piston pressure amplitude was within 3% of the value of the asymptotic form of the pressure amplitude, and marked by the black line. It should be noted that the acoustic Far-Field for this transducer was calculated assuming the transducer was operating solely at the 200 kHz center frequency. Since this transducer was actually sending out a broad band LFM pulse the frequency of the transducer was actually ranging from 160 kHz to 260 kHz which could vary the Far-Field slightly from the calculated value above. However, these factors were ignored and the Far-Field distance calculated was assumed to be accurate since it used the median operating frequency of the transducer.

Another property of the acoustic system that needed to be modeled was the beam pattern of the transducer. The beam pattern gives useful insight into the angular position and intensity level of the side lobes which can add noise to the acoustic signal in the tank, as well as the beam width of the main lobe. In order to calculate the beam pattern two equations were used. The first was the equation for the directional factor of the transducer, **Eqn. 3** (Kinsler, 1999: Eq.7.4.18), which gives the angular dependance of the acoustic signal from the transducer.

$$H(\theta) = \left( \frac{2*J_1(ka*\sin(\theta))}{ka*\sin(\theta)} \right) \quad \text{Eqn. 3}$$

$J_1$  in **Eqn. 3** above is a first order Bessel function which can be implemented in matlab using the code `besselj( )`. The  $k$  and  $a$  in **Eqn. 3**, are the same values used to calculate the Far-Field above and the  $\theta$  was a range of transmit angles from -90 to 90 degrees with 0 degrees being the on axis direction of the transducer (directly perpendicular to the flat head of the transducer).

Once the directional factor was determined the beam pattern could then be calculated using the following **Eqn.4** (Kinsler, 1999: Eq.7.6.1).

$$BP(\theta) = 20\log_{10}(H(\theta)) \quad \text{Eqn. 4}$$

This equation converts the normalized directional factor intensity into decibels (dB) which is more convenient for viewing and understanding the beam pattern; the beam width of the main beam and the location and size of the side lobes.

The -3dB beamwidth of the main lobe of the transducer was determined to be 7 degrees, from **Figure 4** above. This corresponds with the beam width given by Simrad in the specs sheet for the transducer, meaning the beam width was calculated

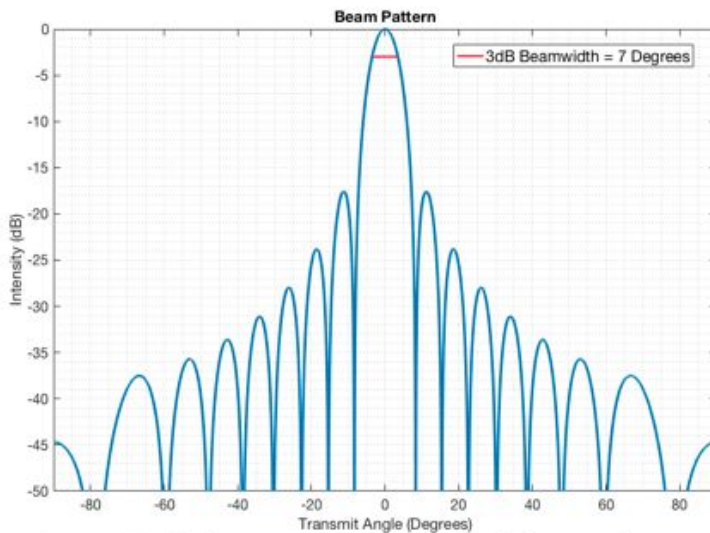


**Figure 4:** The beam pattern (in dB) of the transducer as a function of transmit angle (in degrees).

correctly. The first sidelobes occur at transmit angles of about -11 and 11 degrees, with an intensity of about -18 dB. This information can be useful when determining the necessary tank dimensions (diameter or width/length) to ensure that there is no sidelobe interference in the tank.

## 2.2 Initial Acoustic Pulse Model

In order to model the acoustic pulse response from the ice, a model for the initial broadband pulse that the transducer creates must be created. Using the EK80 transceiver software the transducer was programmed to produce a  $0.512\text{ ms}$  long linearly frequency modulated (LFM) pulse, with frequency band ranging from  $160\text{ kHz}$  to  $260\text{ kHz}$ . The model created used the complex exponential acoustic wave solution for an LFM pulse shown below in **Eqn. 5**.

$$P_{LFM} = AP_o e^{j2\pi\left(f_o + \frac{(f_f - f_o)}{2\tau}t\right)} \quad \text{Eqn. 5}$$

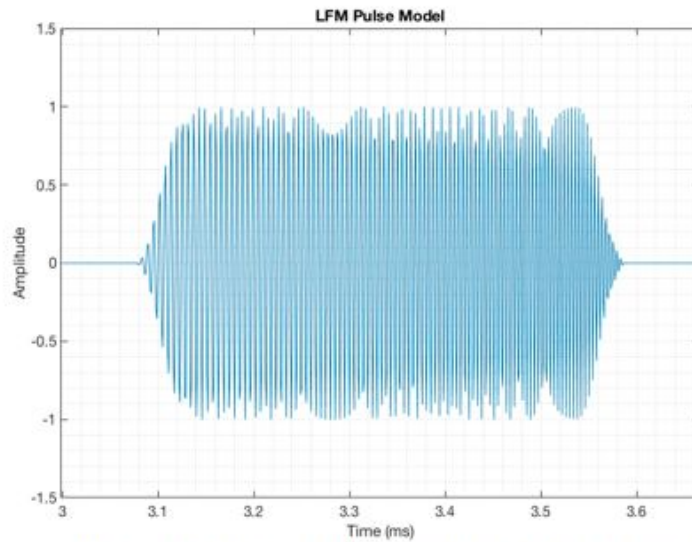


**Figure 5:** The model of the linearly frequency modulated,  $0.512\text{ ms}$  long pulse used for the project.

In the equation above  $A$  is a shading function used to shape the pulse,  $P_o$  is the initial pressure amplitude,  $j$  is  $\sqrt{-1}$ ,  $f_o$  and  $f_f$  are the initial and final frequencies of the pulse/transducer respectively,  $\tau$  is the pulse length and  $t$  is the time span this pulse is being modeled over. For the model used in this experiment a tukey window shading function was used (in Matlab, `tukeywin( )`),  $P_o = 1\text{ kPa}$ ,  $f_o = 160\text{ kHz}$ ,  $f_f = 260\text{ kHz}$ ,  $\tau = 0.512\text{ ms}$  and  $t$  ranged from  $0$  ms to  $6.67\text{ ms}$ .

The implementation of the tukey window function not only shaped the pulse (tapering the ends) but it also reduced the effects of side lobes. This made the model more accurate because the transducer also used a tukey window shading function to reduce side lobe effects as well. It can be seen in **Figure 5** that the LFM pulse starts at a lower frequency and increases over its duration to a higher frequency meaning the LFM part of the model was correctly calculated.

Once the LFM pulse was modeled in the time domain, a Discrete Fourier Transform was performed on the pulse signal in Matlab by `fft( )`, to determine its frequency content/distribution as well as to convert the pulse model from the time domain into the frequency domain for later mathematical manipulation.

It can be seen in **Figure 6** that the frequency distribution of the LFM pulse ranged from 160 kHz to 260 kHz, roughly centered around 200 kHz which was why the transducer was classified as a 200 kHz transducer, even though it used a broad band pulse. The broad band LFM pulse was used for this project to increase resolution of the ice thickness through improving accuracy of the matched filter run on the reflected pulse data. This process will be discussed in further detail below.

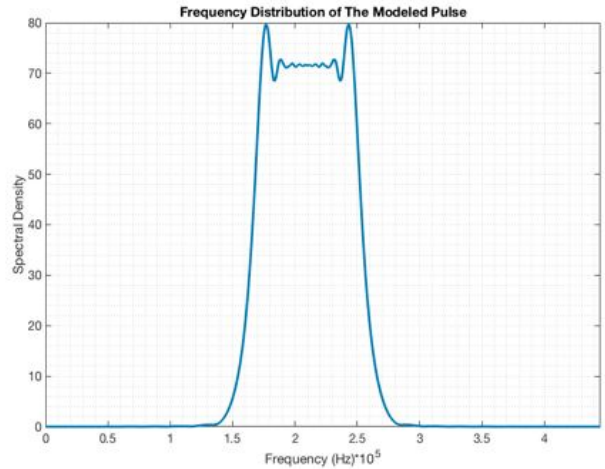


**Figure 6:** The FFT of the LFM pulse signal, showing the frequency content and distribution.

### 2.3 Modeling Boundary Interactions/Ice Thickness

Once the pulse was modeled the model for the reflection coefficient or the reflected pulse signal being received by the transducer needed to be generated. The reflection and transmission model must take into account the physical boundaries/properties of the water/ice and ice/air interfaces. The two properties that must be known are the density and sound speed properties of each medium that the acoustic pulse is propagating through in order to calculate the correct acoustic impedance at each boundary layer. The basic boundary layer diagram used to solve for the reflection coefficient is shown in **Figure 7**.

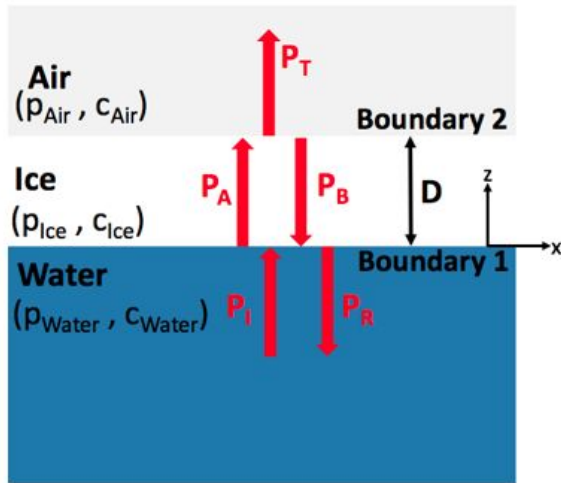


**Figure 7:** A diagram of the reflection and transmission process through a layer of ice with thickness D.

The red arrows and accompanying  $P$ s in the diagram represent the incident, reflected and transmitted acoustic wave pressures at each boundary layer. The distance  $D$  is the thickness of the ice layer and the origin on the diagram depicts that the bottom of the ice for this model is at  $z=0$  and the top of the ice is at  $z=D$ . To produce this reflection coefficient model the complex exponential plane wave solution to the acoustic wave equation (**Eqn. 6** below) was implemented (Kinsler, 1999).

$$P_N = NP_I e^{jkz} \quad \text{Eqn. 6}$$

The plane wave solution was used because in the Far-Field where the ice is growing the acoustic wave signal can be modeled as a plane wave. The  $N$  in **Eqn. 6** above represents the reflection or transmission coefficient (R, A, B and T) in the diagram,  $P_I$  is the initial pressure

amplitude of the incident wave, the  $\pm$  is included to take into account the direction of the wave propagation (up is -, down is +),  $k = \frac{2\pi f}{c}$  is the wave number in each medium, where  $f$  is the range of frequencies used in the pulse model above,  $c$  is the speed of sound through the particular medium, and  $z$  is the vertical distance. Using this information 5 pressure equations for each of the reflected, transmitted and incident waves as a function of both frequency and ice thickness can be created and are shown below in **Eqn. 7**.

$$\left. \begin{array}{l} P_I = P_I e^{-jk_{water}z} \\ P_R = RP_I e^{jk_{water}z} \end{array} \right\} \begin{array}{l} \text{Water} \\ \text{Layer} \end{array} \quad \left. \begin{array}{l} P_A = AP_I e^{-jk_{ice}z} \\ P_B = BP_I e^{jk_{ice}z} \end{array} \right\} \begin{array}{l} \text{Ice} \\ \text{Layer} \end{array}$$

$$P_T = TP_I e^{-jk_{air}z} \left. \vphantom{P_T} \right\} \begin{array}{l} \text{Air} \\ \text{Layer} \end{array}$$

**Eqn. 7**

Once all the pressure equations for each boundary were derived, with the 4 unknowns  $A$ ,  $B$ ,  $T$  and  $R$ , 4 equations were created using these 5 pressure equations to solve for the unknowns. The 4 equations were created using two boundary conditions applied at each boundary layer according to the following two governing equations. The first equation was the continuity of pressure at each boundary, whose basic form is shown below (**Eqn. 8**).

$$P_I + P_R = P_T \quad \text{Eqn. 8}$$

In **Eqn. 9** it is clear that the pressure on one side of the boundary layer must equal the pressure on the other side of the boundary layer. The second governing equation is the continuity of normal particle velocity at each boundary, whose basic form is shown below in (**Eqn. 9**).

$$\overline{U}_I + \overline{U}_R = \overline{U}_T \quad \text{Eqn. 9}$$

It is also clear in **Eqn. 9** above that the normal particle velocity on one side of the boundary layer must equal the normal particle velocity of the other side of the boundary. The normal particle velocity of the acoustic wave is directly related to the pressure of the acoustic wave shown below in **Eqn. 10** (Kinsler, 1999).

$$\overline{U}_N = \frac{NP_I}{\rho c} e^{\pm jkz} \hat{z} \quad \text{Eqn. 10}$$

The equation for the normal particle velocity (**Eqn. 10**) is a vector equation as depicted by the  $\overline{U}_N$  and  $\hat{z}$  the unit vector of the velocity direction. The  $N$ ,  $k$  and  $z$  are the same variables as the ones above in the pressure equation,  $\rho$  is the density of the medium and  $c$  is the speed of sound in the medium. The resulting normal velocity equations for each of the reflected, transmitted and incident waves are shown below in **Eqn. 11**.

$$\left. \begin{array}{l} U_I = \frac{P_I}{\rho c} e^{-jk_{water}z} \hat{z} \\ U_R = \frac{-RP_I}{\rho c} e^{jk_{water}z} \hat{z} \end{array} \right\} \begin{array}{l} \text{Water} \\ \text{Layer} \end{array} \quad \left. \begin{array}{l} U_A = \frac{AP_I}{\rho c} e^{-jk_{ice}z} \hat{z} \\ U_B = \frac{-BP_I}{\rho c} e^{jk_{ice}z} \hat{z} \end{array} \right\} \begin{array}{l} \text{Ice} \\ \text{Layer} \end{array}$$

$$U_T = \frac{TP_I}{\rho c} e^{-jk_{air}z} \hat{z} \left. \vphantom{U_T} \right\} \begin{array}{l} \text{Air} \\ \text{Layer} \end{array}$$

**Eqn. 11**

The negative sign in front of  $U_R$  and  $U_B$  are a result of the velocity equation being a vector equation and the normal particle velocity for those two wave fronts are in the negative direction. Once all of the pressure and normal particle velocity equations were determined for each reflected, transmitted and incident wave, the equations can be plugged into the 2 governing equations for continuity or pressure and normal particle velocity at each boundary. These equations were then evaluated at the correct  $z$  distance, which according to the reflection and transmission diagram above (**Figure 6**), the water/ice boundary layer is at  $z=0$  meters and the ice/air interface is at  $z=D$  meters.

Once the 4 boundary equations were evaluate at both  $z=0$  and  $z=D$  they were simplified and the equations formed a system of 4 equations with 4 unknowns ( $A$ ,  $B$ ,  $R$  and  $T$ ) (**Eqn. 12**).

$$\begin{array}{l}
 \text{Continuity of Pressure} \\
 \text{Continuity of Normal Particle Velocity}
 \end{array}
 \left\{ \begin{array}{l}
 R - A - B = -1 \\
 Ae^{-jk_{ice}D} + Be^{jk_{ice}D} - Te^{jk_{Air}D} = 0 \\
 -R - \frac{\rho_{Water}c_{Water}}{\rho_{Ice}c_{Ice}} A + \frac{\rho_{Water}c_{Water}}{\rho_{Ice}c_{Ice}} B = -1 \\
 Ae^{-jk_{ice}D} - Be^{jk_{ice}D} - T \frac{\rho_{Ice}c_{Ice}}{\rho_{Air}c_{Air}} e^{jk_{Air}D} = 0
 \end{array} \right.
 \begin{array}{l}
 \text{(Water/Ice)} \\
 \text{(Ice/Air)} \\
 \text{(Water/Ice)} \\
 \text{(Ice/Air)}
 \end{array}$$

**Eqn. 12**

This system of equations could be converted into matrices and solved at varying thicknesses ( $D$ ) and frequencies, with the same range of frequencies that was used to create the frequency distribution of the pulse model. Then the system of equations could be solved with the backslash matrix operator to determine the reflection and transmission coefficients of  $R$ ,  $A$ ,  $B$  and  $T$ , (**Eqn. 13**).

$$\begin{pmatrix}
 1 & -1 & -1 & 0 \\
 -1 & -\frac{\rho_{Water}c_{Water}}{\rho_{Ice}c_{Ice}} & \frac{\rho_{Water}c_{Water}}{\rho_{Ice}c_{Ice}} & 0 \\
 0 & e^{-jk_{Ice}D} & e^{jk_{Ice}D} & -e^{jk_{Air}D} \\
 0 & e^{-jk_{Ice}D} & -e^{jk_{Ice}D} & -\frac{\rho_{Ice}c_{Ice}}{\rho_{Air}c_{Air}} e^{jk_{Air}D}
 \end{pmatrix} * \begin{pmatrix} R \\ A \\ B \\ T \end{pmatrix} = \begin{pmatrix} -1 \\ -1 \\ 0 \\ 0 \end{pmatrix}$$

**Eqn. 13**

Since the data recorded by the transducer was only from the received reflected pulse signal the only coefficient of significance for this project was the reflection coefficient. So the reflection coefficient,  $R$ , was solved for as a function ice thickness and frequency in Matlab.

## 2.4 Received Pulse Prediction

Once a solution for the reflection coefficient/reflected pressure as a function of both frequency and ice thickness was determined, the reflected pulse response could then be modeled. This was done by multiplying the fourier transformed pulse model (in the frequency domain), by the solution for the reflection coefficient as a function of both frequency and ice thickness. This solution was then inverse fourier transformed to convert the answer back into the time domain.



Next a matched filter was performed on the initial pulse created and the determined reflected pulse both in the time domain to determine the predicted pulse response as a function of ice thickness. The matched filter used a linear correlation between the initial pulse created and the modeled reflected pulse, in Matlab by “*corr(x,y)*”. Once the matched filter was performed the pulse response solution for different ice thicknesses could then be plotted and compared to the actual pulse response from the acoustic data.

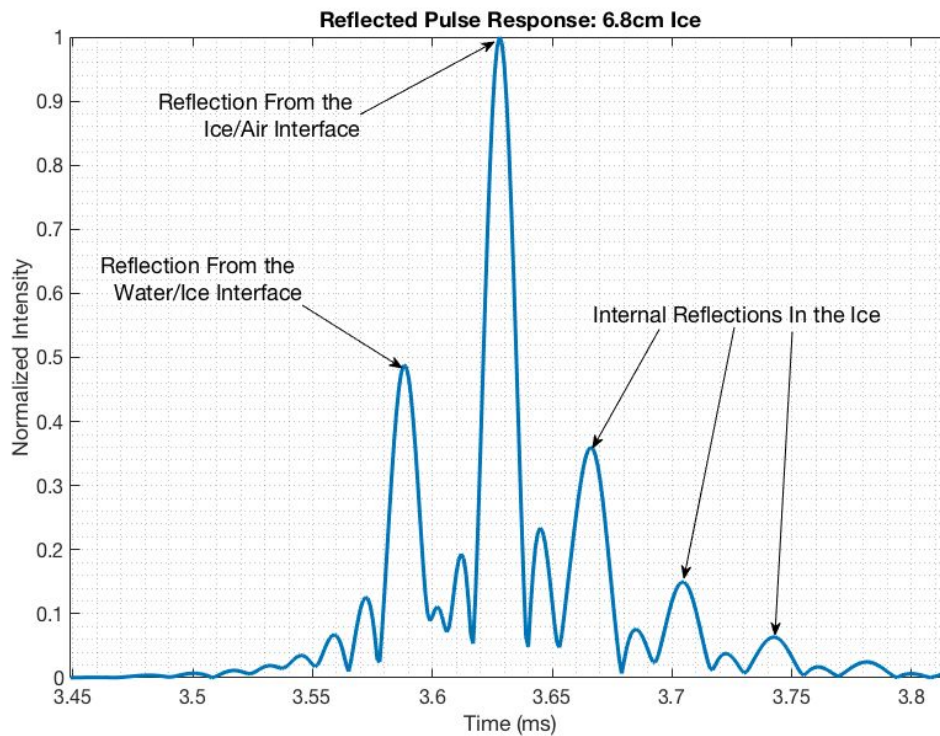


**Figure 8:** The prediction for the received reflected pulse response with an Ice thickness of 6.8 cm.

The first reflected pulse received on the left is the reflection from the water/ice interface (as labeled), the second reflected pulse is the reflection from the ice/air interface (as labeled). It is clear that the reflection from the ice/air interface is much stronger in intensity than the reflection from the water/ice interface. This is due to the fact that the acoustic impedance between the ice/air interface is much stronger than the acoustic impedance between the water/ice interface. The magnitude difference due to the acoustic impedance contrast between the reflections both theoretically and practically makes sense, reinforcing our model. The reflections to the left of the ice/air interface reflection are internal reflections within the ice. There are multiple reflections within the ice layer from the pulse inside the ice reflecting off both the water/ice and air/ice boundaries due to the acoustic impedance contrast at each boundary. By comparing the predicted pulse response to the actual recorded pulse response, the correlation in location and intensity of the different reflections can help to refine the predicted model and resolve any issues with it.

## 3. Design Considerations

### 3.1 Required Instrumentation

The main instrument being utilized in this experiment was a broadband acoustic transducer, specifically the Simrad ES200-7CD, a 200 kHz, split-beam composite transducer.

This transducer was controlled via the Simrad EK80 Wide Band Transceiver (WBT), which allows the user to define settings and operating parameters for the transducer. This equipment was provided at the onset of the project by Dr. Weber.

The design of the main experimental setup called for a large, enclosed, water tank.

Due to the need for a completely encased system in order to prevent heating of the tank interior, it was necessary to install various instruments and sensors within the tank to provide an accurate depiction of what was occurring inside.

In order to provide a temperature profile of both the air and water within the tank, thermistors were potted within a PVC housing at 1” intervals. These thermistors gave temperature readings throughout the tank, which allowed for accurate sound speed calculations in the water column, cooling rate analysis within the tank and approximate ice growth/thickness. A digital temperature probe was also placed inside of the tank to give a comparative measurement of the air temperature.

A fabricated underwater camera was hung in the tank, which monitored the conditions in the tank and the ice growth. A measuring pole was also installed in the tank in hopes of gaining ice thickness measurements from the underwater camera images. An above water camera was also installed in the tank to gain more information on the conditions in the tank, especially above the ice. Waterproof lighting was also placed in the bottom of the tank to illuminate the inside of the tank and allow the two cameras to capture images for analysis and timelapse.

#### 3.1.1 Thermistor Array Construction and Calibration

A total of 12 thermistors were used to provide a temperature profile from the air down through the top 10 inches of ice/water. These top 11 thermistors were epoxied in place through holes in a 1-¼ inch PVC housing, starting 7 inches below the top edge of the tank. Each of these thermistors were spaced at an interval of 1 inch on center. The last thermistor, located 10 inches



**Figure 9:** The Simrad ES200-7CD transducer used throughout this experiment  
(<https://www.simrad.com/www/01/nokbg0240.nsf/AllWeb/3ADE61D37DE79B37C12575430040FE22?OpenDocument>)



away from the vertical pipe of the housing in the horizontal pipe, was placed there to measure the temperature near the tank bottom. This thermistor was approximately 4 inches above the bottom of the tank, close to the depth of the transducer. This thermistor layout and housing is shown below in *Figure 10*.

Before construction, the benefits and disadvantages of NTC, PTC and digital thermistors were compared. The advantages of NTC thermistors are that their resistance decreases as the temperature goes up. However, because the tank is designed to reach a minimum of about  $-10\text{ }^{\circ}\text{C}$ , the high resistance of NTC thermistor might cause self-heating that influences the accuracy and requires more advanced circuit to resolve the measurement. The NTC thermistor was therefore not preferred as a first choice.

PTC thermistors give a solution for the low temperature measurement but introduce issues of their own. If a high density temperature profile is required, several thermistors are required but the Arduino Uno board which is used to control thermistors and collect data limits the number of outputs. The solution is to either find a way to connect thermistors by few outputs or to increase the size of the Arduino control board. Increasing the output of the control board would be quite difficult, therefore it was decided to condense the output of the thermistor array. The circuit was designed as shown in *Figure 11*. However, the disadvantage of it is that the output of the system will be relative differences in voltage, and an extra output is need to report a initial temperature. This requires more than one Arduino Uno board if more than eight sensors are necessary.

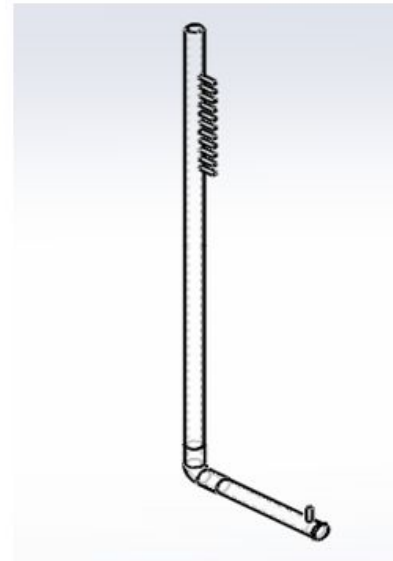


**Figure 10:** The CAD model for the thermistor array and housing which includes 12 DS18B20 digital temperature sensors

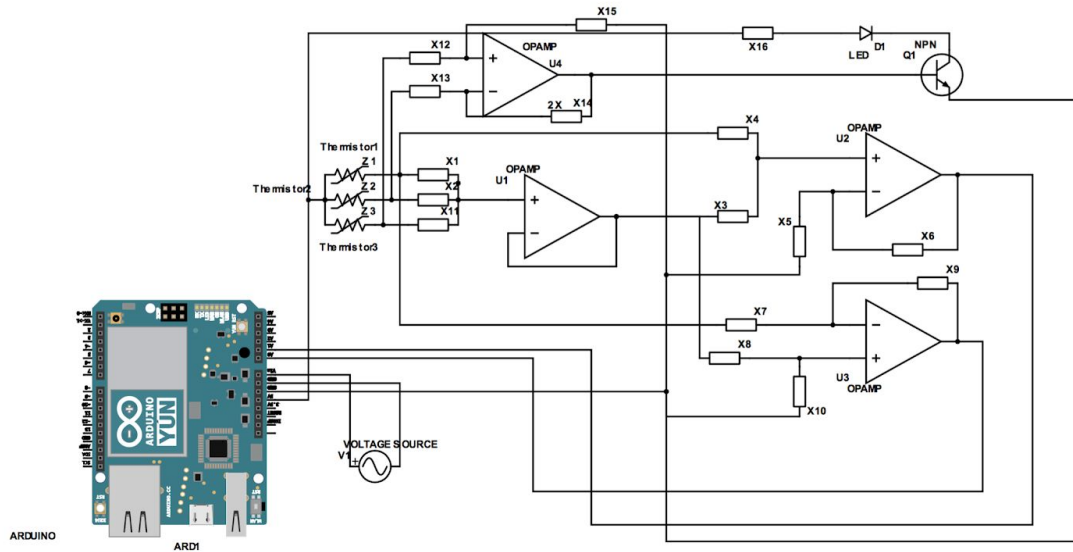


**Figure 11:** The initial circuit design for 3 thermistors to share two outputs, in order to connect multiple thermistors to an Arduino board. However, this circuit is complex and is not effective for a large amounts of thermistors.

Due to the fact that more than six sensors would be necessary in order to form an actual profile, the DS18B20 digital temperature sensor was considered. The DS18B20 sensor give an accurate measurement of temperature ranging from  $-55\text{ }^{\circ}\text{C}$  to more than  $100\text{ }^{\circ}\text{C}$ , while resolution can be adjusted and multiple sensors can share one output through a one-wire system. For this reason, the DS18B20 sensors were utilized. Setup of these sensors was mainly done through coding which avoided the tedious work of calibration. Instead these digital sensors would send out the temperature directly. For this temperature instrument 2 one-wire systems were used with 2 digital outputs of Arduino Uno board while each was connected with 6 sensors in parallel with a 4.7k resistor. Although the temperature would be reported directly by the system, the accuracy and stabilization of the sensors required a check to understand the error of this temperature instrument.

The accuracy of the sensors was analyzed before potting them in the array to ensure they were operating correctly. This was done by comparing the thermistor measurements to those obtained via a handheld temperature probe. The collected data showed that there were deviations between sensors when taking simultaneous measurements. Due to this, an analysis of variance was used to determine if there was a significant measurement difference between these 12 sensors. A total of 120 data points were collected to compare these measurements by subtracting the temperatures collected by sensors from the temperatures measured by the probe. The sensors were put together with the probe both inside lab and outside the laboratory building door 5 times, and each time as allowed for equilibration.

From the overlay plot shown in *Figure 12*, the collected data distributed randomly without obvious patterns. This showed that the sensors were stable and independently worked while sharing the one-wire systems.

The normal quantile plot shows the assumption of normality was reasonable, the deviation of temperature above 0 °C is shown separated from that of below 0 °C as shown in *Figure 13*.

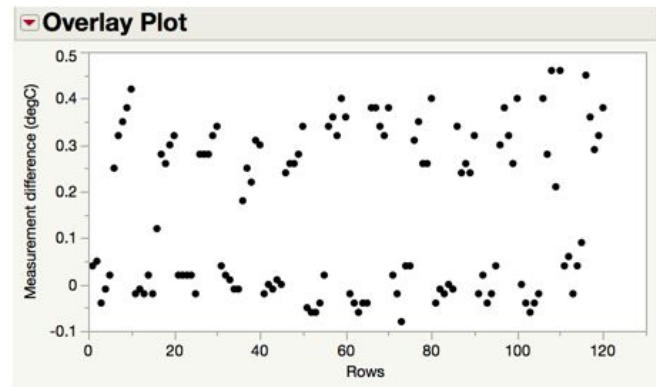


**Figure 12:** The overlay plot by JMP for a total 120 data points of measurement differences between the data collected by 12 temperature sensors and the corresponding thermometer data. Half of them are above 0 °C while the other half are below.

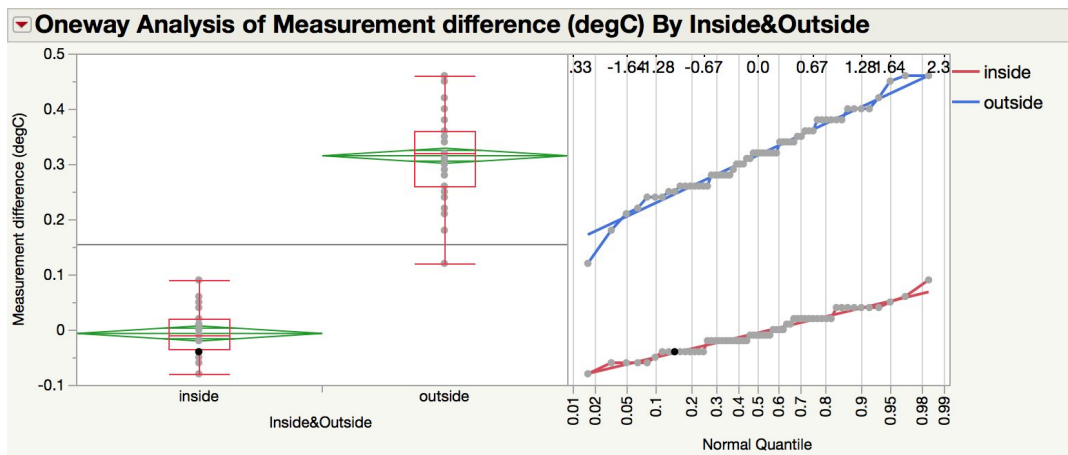


**Figure 13:** The left plot is the deviations of 12 sensors compared with the thermometer at temperatures above and below 0 °C. The inside group includes deviations at temperature higher than 0 °C, while outside group includes deviations at temperature lower than 0 °C. The right plot is the normal quantile plot for the deviation data, plotted by JMP, in which data points are distributed near the linear fit line, showing that for each group, sensors work independently although the measurement deviation varies with temperature above and below 0 °C .

A resolution of 0.06 °C for the sensors and a resolution of 0.1 °C of the temperature probe caused a fixed deviation difference between the measurements. Due to the data being collected outside for a low temperature measurements, the temperatures measured below 0 °C range from -8.6 °C to -4.5 °C. In comparison above zero temperatures were collected ranging from 2.3 °C to 18.9 °C. The measurements were taken for approximately three minutes to allow for equilibration. *Figure 14* below shows a general response of sensors to a temperature below 0 °C.

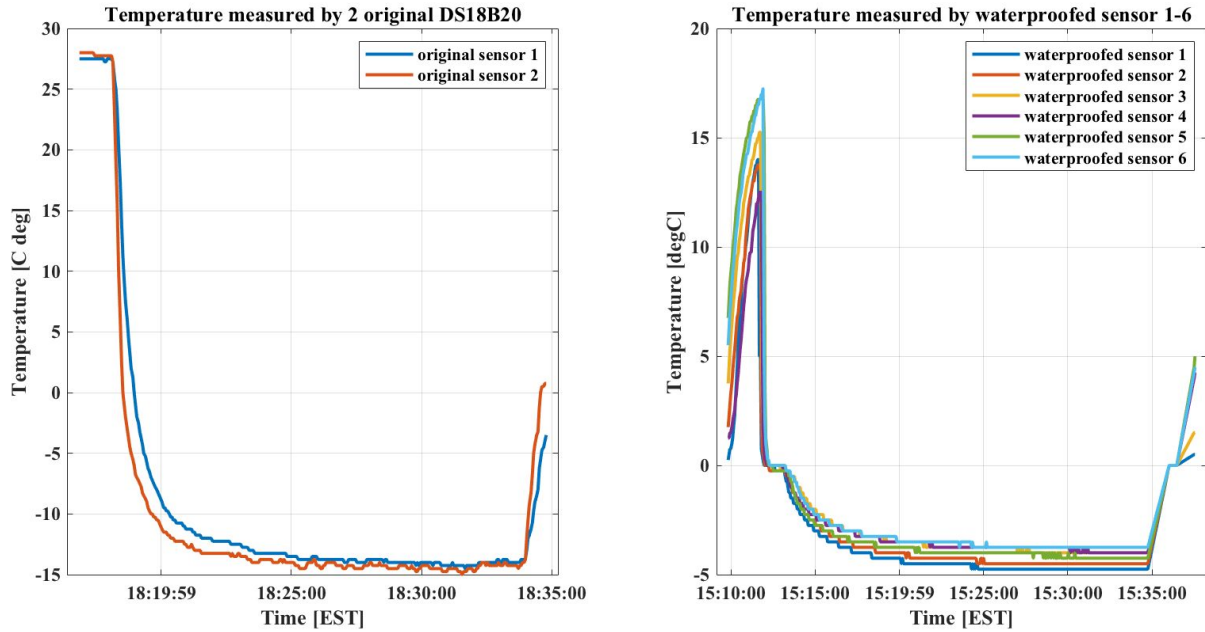


**Figure 14:** These plots show the temperature responses to a range of temperatures from about  $-15^{\circ}\text{C}$  to  $28^{\circ}\text{C}$ , by the original 2 sensors and the waterproofed 6 sensors in stainless steel housings, respectively.

In the left plot, the original DS18B20s was placed outside the laboratory building door until a steady temperature was reached. This was done in mid-February at a time when it was cold and windy. In the right plot, 6 waterproof DS18B20 sensors sharing a one-wire system were put in a tub of snow at slightly different places and depths without mixing after being shortly exposed to room temperature.

The deviations between the 12 sensors are not statistically significant as shown by the analysis of variance in **Figure 15**. Overall, the thermistor array measured temperature with an accuracy of  $0.16^{\circ}\text{C} \pm 0.17^{\circ}\text{C}$  when compared with the thermometer.

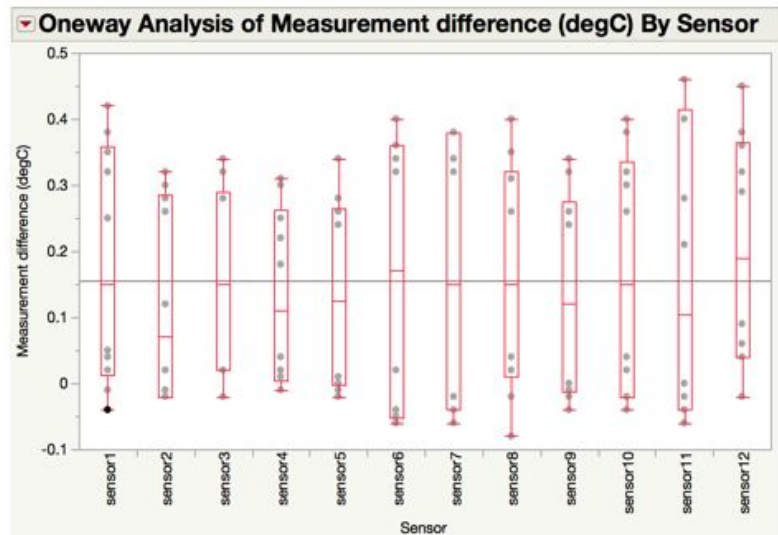


**Figure 15:** The box plot for the deviations of each of 12 sensors compared with the thermometer at all measured temperatures by JMP.

## 3.2 Initial Sizing, Insulation and Cooling Needs

### 3.2.1 Acoustic Near-Field Considerations

An important factor to consider when deploying an acoustic device is distance until the far field of the acoustic beam is reached. In the near field, a mixing of propagating and circulating waves occurs causing a complicated interference pattern. This makes the signal in the near field difficult to predict and analyze. In the far field however this interference pattern ceases and the radius of the propagating acoustic wave can be considered large enough that the signal is modeled as plane wave with no curvature. At this distance the wave can also be considered to be propagating only, rendering a clear return signal from the target that can be modeled. The far-field distance for this transducer as discussed above in the Acoustic Theory and Predictions section was calculated at a distance of 0.45 m. This meant that the tank had to be large enough for the transducer's head to be a minimum of 0.45 m away from the bottom of the ice. It was decided that the tank should be a minimum of 1 m in depth in order to achieve this spacing for the far-field with a significant amount of ice grown.

Another important consideration that was used for sizing the tank was the interaction of side lobes in the received signal. The tank had to be wide enough so that the dominant side lobes' signal would not reflect back off the sides of the tank and the edges of the ice before the main lobe's signal traveled through the ice and reflected back to the transducer directly above the transducer. Properly sizing the diameter or width of the tank would reduce or eliminate side lobe interference decreasing noise in the received signal. Using this information, along with approximate sound speeds through water and ice, and the 1 m tank depth previously determined, basic acoustic geometry was performed. A diameter or width of about twice the depth, 2 m, was deemed suitable for preventing side lobe interaction. This meant that the transducer should be roughly the same distance from the bottom of the ice as it would be from the walls of the tank.

### 3.2.2 Heat Transfer Overview

The tank had to be a well insulated closed system in order to freeze water inside with room temperature conditions outside of the system. With an approximate tank size as large as discussed above, there would be a large amount of heat transfer into the tank from the heat in the room, which would need to be opposed by enough insulation and a high enough capacity cooling system. To determine both insulation amounts and cooling system capacity, the ideal conditions for ice growth and optimal ice thickness within the tank had to be determined. These conditions differed depending on the tank design, since 3 different tank designs were created throughout the course of this experiment. However, throughout all the different tank designs, the method for calculating the heat transfer into the tank from the hotter room temperature air outside of the tank remained the same. The conductive heat transfer equation (*Eq. 14* below) was used to determine the net heat transfer into the closed tank system.

$$Q = \frac{kA(T_2-T_1)}{d} \quad \text{Eq. 14}$$

In the conductive heat transfer equation above  $k$  is the thermal conductivity of the material which heat is being transferred through,  $d$  is the thickness of the material and  $A$  is the area which heat is being transferred through.  $T_2$  is the temperature inside the tank and  $T_1$  is the temperature outside of the tank, which means the equation will calculate the amount of heat transferred into the tank from the room temperature air. Since the majority of insulation material's properties in the US are given as imperial R-values (thermal resistance) as opposed to metric k-values (thermal conductivity), it was useful to rewrite **Eq. 14** above to use the R-value equivalents for insulation. The R-value or  $R$  is equal to **Eq. 15** below, where  $k$  and  $d$  are the same values as explained above.

$$R = \frac{d}{k} \quad \text{Eq. 15}$$

By combining **Eq. 14** and **Eq. 15** the following equation which used R-value as opposed to k-value and thickness was created (**Eq. 16** below).

$$Q = \frac{A(T_2-T_1)}{R} \quad \text{Eq. 16}$$

This conductive heat transfer equation above was used throughout the majority of the project due to the fact that R-value information were more readily available than k-value information for the materials used. This also meant that the majority of the net heat transfer calculations were calculated in imperial units and then converted into metric units.

### 3.2.3 Insulation Considerations

The original heat transfer calculations were done based on a much larger tank that was initially being considered as the tank for this experiment. These initial heat transfer calculations helped determine the approximate insulation needs and the cooling system capacity needed to achieve the project goals. The insulation and cooling system were determined through multiple iterations of designs and calculations. Through this iterative process the designs became more refined and more efficient. The three main insulation materials used throughout all 3 designs were reflective bubble wrap insulation, fiberglass batt insulation and polyisocyanurate foam board insulation. These insulation types were chosen for a variety of factors each.

For the first round tank design the reflective bubble wrap insulation and flexible fiberglass batt insulation were chosen due to their ability to be wrapped around the sides of the tank. In general for all the designs, the reflective bubble wrap insulation cut down on condensation on the outsides of the tank walls which would reduce losses through the tank walls. Also, The 9in fiberglass had a high, R-value of  $30 \frac{ft^2 \cdot ^\circ F}{Bth/hr}$  that would be advantageous for all the tank designs. The polyisocyanurate foam board also had a high R-value of  $13 \frac{ft^2 \cdot ^\circ F}{Bth/hr}$  per 2 inch thick board and it was useful for making a rigid top that was removable and sealed the tank from air leaks. However, it was the most expensive form of insulation used in all of the designs.

Since the initial tank design was based off of a much larger cylindrical tank (height = 65", D = 86") than any of the subsequent tank designs, the initial calculations for heat transfer through the insulated walls were essentially maximized. The steady state conditions within the tank were also set to be at a minimum temperature based on the minimum temperature residential freezers could achieve. This meant that the air and ice in the original tank design were modeled to be 0 °F or -18 °C, the water was 39 °F or 4 °C and the air surrounding the system at room temperature was 77 °F or 25 °C. These internal steady state temperatures were much lower than subsequent design conditions and were adjusted due to their impracticality. However calculating on the initial heat transfer using the coldest temperatures possible also allowed for a greater factor of safety when sizing the cooling system.

A complete overview of the original design used to determine approximate insulation amounts and cooling system output are as follows; two layers of reflective bubble wrap insulation and one layer of 9 inch fiberglass batt insulation around the sides of the tank. Two 1 in plywood sheets sandwiched around 4 inch of polyisocyanurate foam board on top and 6 inch of cork insulation on bottom to support the wait of the fully insulated tank. This insulation design, along with the internal conditions and the use of the conductive heat equation explained above, resulted in an initial heat transfer into the tank of around 454 Btu/hr or 133 W. However this tank was never obtained due to the shipping wait time and the design had to be adjusted.

### 3.2.4 Cooling System Requirements

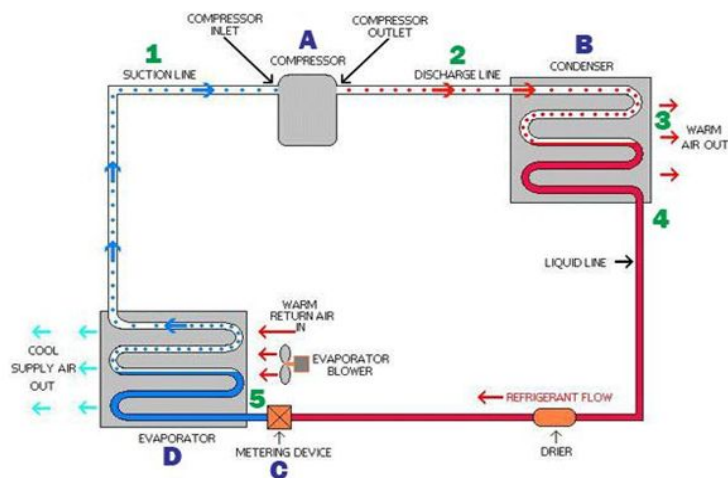


**Figure 16:** A diagram depicting how a freezer system operates and components within its system (<http://www.air-conditioning-and-refrigeration-guide.com>)

In order to create the conditions under which ice would freeze in this water tank, a method of constantly providing cooling power needed to be implemented. This system needed to be powerful enough to cope with the cooling losses from (or the heat transfer into) the tank discussed above while maintaining below freezing temperatures. Based on the analysis for the heat transfer of the first tank design, it was determined that a system capable cooling at the rate of at least 600 Btu/hr would be required. Although a cooling system custom built for the tank would be best, budget constraints dictated that an existing system be obtained and

modified to fit the design parameters.



As it was decided that an existing system be obtained and modified, it was necessary to find which type would be best. Two separate freezer units were discussed and the benefits and shortcomings of each were discussed. The first system considered was a self contained, commercially available, walk in freezer unit. This system could be mounted directly to the tank and would most likely have more than enough power to handle sub zero temperatures for the duration of the experiment. These units are costly however, with used systems falling in the \$2000-\$5000 dollar range. They are also fairly complicated, and repairs often require experienced technicians.

The second option discussed was modifying a chest freezer to perform the necessary operation. This would be done one of two ways. The first option would be constructing a system to circulate air between the freezer and the inside of the water tank, using the inside of the chest freezer as a space to cool the circulated air. If this did not properly work the freezer would be deconstructed and an attempt to salvage the internal components (e.g. compressor, condenser, and evaporator coils) would be made. If these components could be removed intact, then the coils would be bent to fit within the fabricated lid of the tank. If they became damaged in the process, then copper piping would be used to create new condenser/evaporator coils suited to size of the tank. The compressor would then need to be recharged per the manufacturer's specification.

Due to budget constraints, the method centered around a chest freezer was utilized. The model bought was a 10.2 cubic foot standard chest freezer which operated at 115 Volts and 130 Watts. The compressor driving the system was listed as  $\frac{1}{3}$  HP, which gives a conservative cooling output of 667 Btu/Hr. This was based on a combination of sources which listed horsepower to Btu/hr conversions, and using a conservative estimate of 1 HP = 2000 Btu/hr Freezing. This system was determined to be the optimal balance between cost and cooling power, and gave options for modification.

## **4. Designs and Modifications**

The initial tank design discussed in section 3.2 (Initial Sizing, Insulation and Cooling Needs), was used as a starting point for sizing, insulation amounts, cooling capacity and pricing, but not used as serious design since it was never actually ordered. The tank designs discussed in this section were those for tanks that were either ordered or obtained. Over the course of this project, the design and construction of the insulated water tank and subsequent cooling system went through several variations. Each had its own merits and flaws, as well as unique design requirements.



## 4.1 Version 1

### 4.1.1 Design Description

Throughout the initial design process, it was decided that a large, round water tank would be the preferred setup for this experiment. A smooth, round walled, vessel would help to minimize acoustic noise in the received signal from a bottom mounted transducer, given that the tank was large enough and that the width of the main acoustic beam was kept to a minimum. Knowing this, a 750 gallon cylindrical polyethylene tank (60 inches in depth and 60 inches in diameter) was chosen due to both its size and inclusion of a bolt on lid.

Due to the size of this tank being so large, it was imperative to determine the insulation needs required to maintain below freezing temperatures in the tank. Estimates of the losses in the tank were estimated using the conductive heat transfer equation and thermodynamic material properties in order to find the correct insulation amounts for the system. The calculations were based off our ideal steady state tank conditions with an ice thickness of 25 cm at  $-18^{\circ}\text{C}$  degrees, a water depth of 1 meter at  $4^{\circ}\text{C}$  and a 0.4 meter high air pocket on top cooled by the freezer system to  $-18^{\circ}\text{C}$  degrees. Without any insulation and these conditions the tank would experience losses of around 3000 Btu/hr. Next enough insulation had to be added all around the tank to combat these losses enough for the given freezer system to effectively cool the large thermal mass of water in the tank.

In order to insulate this tank to allow for ice growth, multiple layers and varieties of insulation were utilized in the design. A first layer of reflective thermal insulation foil was wrapped around the tank itself. This foil both insulated the tank and mitigated condensation due to its reflective properties. Surrounding this was a single layer of high R-value (R-30) 9 inch thick fiberglass insulation. Outside of this fiberglass would be another layer of thermal foil. The tank itself would sit upon a thick mat made of either rubber or cork to prevent conduction into the concrete floor. Once fully insulated this tank had calculated a net heat transfer of about 300 Btu/hr.

### 4.1.2 Design Flaws

After all calculations and cost analysis were completed, this tank and all the insulation beside the bottom insulate was ordered. Unfortunately this tank was damaged during shipment rendering it unusable on arrival. As this was over winter break and not all of our team members were readily available, our project advisor Dr. Weber, made the decision to order a local tank which deviated further from our original design but would still be useable.

## 4.2 Version 2

### 4.2.1 Design Description

This new and final water tank is a square sided 4 ft x 4 ft x 5 ft polyethylene tank. This tank being square and without an included lid required more design input. To begin with, when filled with water the tank walls and bottom significantly bowed out. The strength of the tank walls was not enough to support the weight of the water and had to be reinforced. After emptying the tank of water, a combination of 2" x 4" boards and industrial ratchet straps were used to pull the tank back into shape. These straps were left in place behind the insulation in order to ensure that the tank did not deform when refilled with water. As the bottom of the tank was also bowing underneath, 2" x 4" boards were used to reinforce this area as well.

In order to insulate the top of the tank, a lid was built using a base of plywood. Surrounding the bottom of this plywood was a rim of 2" x 4"s to create a tight seal around the edge of the tank. On top of the plywood was two layers of 2" thick polyisocyanurate foam insulation. All cracks were filled with quick expanding foam insulation to prevent air leaks and heat losses.

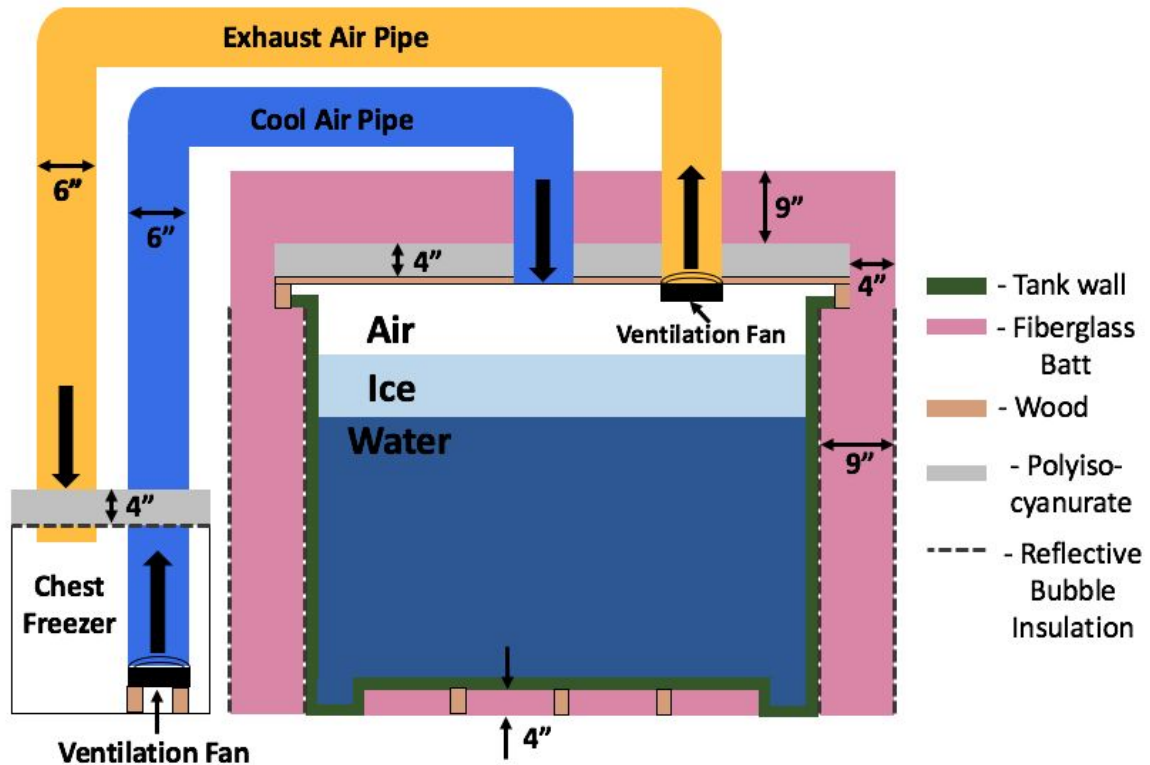


*Figure 17:* The diagram showing the insulation amounts and cooling system setup for the tank design version 2.

The exterior insulation for the tank was assembled per the original plan, with the one variation being the use of fiberglass insulation underneath. Given that this tank rests on 2 feet spanning the length of the tank, there was about a 4 inch space to put fiberglass sheet insulation in the spaces underneath the tank, between the concrete floor and the tank. The sides were insulated using the methods mentioned above, following the layering methods listed, and all layers attached using a combination of industrial adhesive and insulation tape. Additional 9 inch fiberglass batt insulation was also stacked on top and around the lid to add more insulation on top of the tank.



**Figure 18:** The tank and insulation attached to the sides of the tank for design version 2.

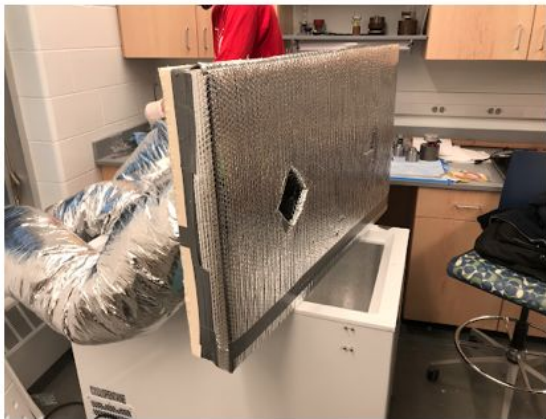


**Figure 19:** The insulated top fabricated for the chest freezer with ventilation pipes attaches

The cooling system was designed in such a way that the chest freezer would remain relatively intact. This was done by first constructing a new, insulated, lid for the freezer.

This new lid had two 6-inch holes cut into it, to which was attached insulated ventilation hoses. These hoses were then attached to the lid of the water tank with ventilation fans attached in order to circulate air throughout the system. It was believed that with the chest freezer operating at maximum power and with enough circulation, the system would be able to achieve below freezing temperatures within the water tank.

The heat transfer calculations performed for this design only took into account the heat transfer into the system through the insulated tank, and not through the chest freezer or through the insulated 6" ventilation piping. The heat transfer calculations performed under these conditions for this tank design yielded a result of around 250 Btu/hr of cooling losses from (heat transfer into) the tank which was thought to be easily combated by the roughly 667 Btu/hr output of the chest freezer cooling system.



**Figure 20:** The final setup of the tank design version 2.

### 4.2.2 Trial Results

When the system was assembled, a trial of the freezing capabilities of the system was run. The temperature profile in the tank was recorded by the thermistor array, and the results were plotted against time. The profile for this trial run can be seen below in **Figure 21**.

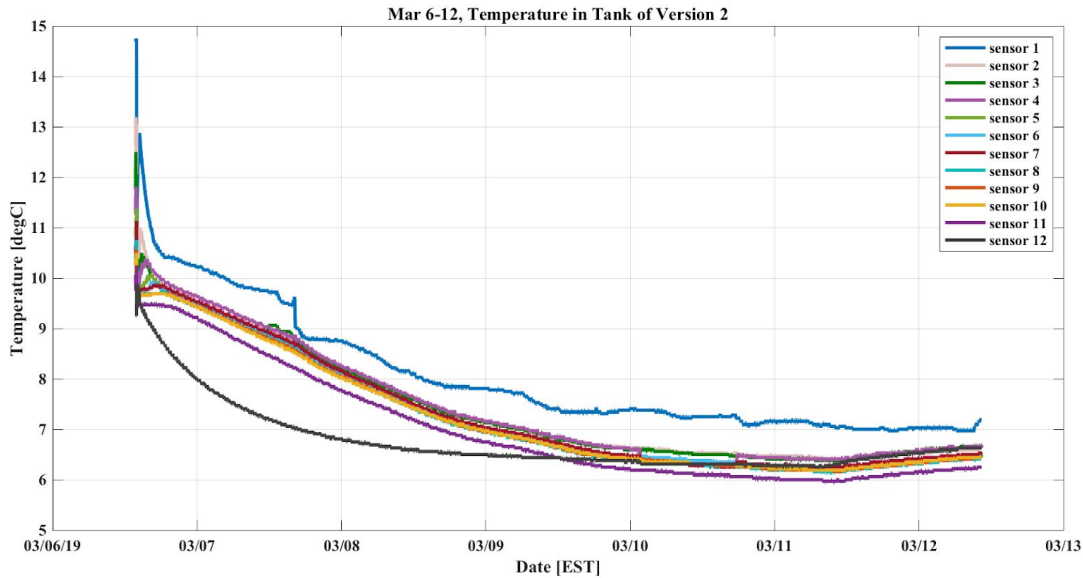


**Figure 21:** The temperature profile for the trial test for tank version 2, which started from Mar 6, 2019 and ended at the noon of the Mar 12, 2019.

The sensor numbers correspond to their location/depth within the tank, starting with sensor 1 in the air and descending to sensor 12 at the bottom of the tank. It can be seen that during this trial run, the temperatures in the system did not reach below freezing, and instead plateaued at 6.5°C. Due to this not being the desired result, the flaws in the system needed to be examined.

### 4.2.3 Design Flaws

As the trial run was unsuccessful, the flaws of the design were evaluated. First, it was determined that there were likely to many losses in the cooling system loop. Although the walls of the freezer reached freezing and accumulated ice, the temperature within the freezing chamber never reached below 1°C. This indicated that the compressor in the freezer was not powerful enough to keep up with the combined air mass of the freezer, venting hoses, and water tank.

Along with the current freezing system not being sufficient, it was determined that there were substantial heat transfer through the bottom of the water tank into the concrete floor. Simply by feeling the floor in lab below the tank, it was found that a significant amount of

cooling was being lost by conduction out of the tank bottom. For both of these reasons, it was decided that a design revisit was required.

#### 4.2.4 Design Revisit

For this design it was decided to revamp both the cooling system and the tank insulation. The tank was drained of water all attached insulation was stripped from the sides and bottom, and the constructed top was discarded. The cooling system was also completely disassembled, with hope of gutting the chest freezer in order to salvage its internal components. New insulation was ordered for the tank, and a new design was drawn up.

### 4.3 Version 3

#### 4.3.1 Design Description

The new tank design had much more insulation of the sides and bottom of the tank where the majority of heat transfer was believed to have originated in the previous tank design. On top of the increase in the amount of insulation, a completely new cooling system was design to minimize losses within the cooling system itself. This new design is shown below in diagram of *Figure 22*.

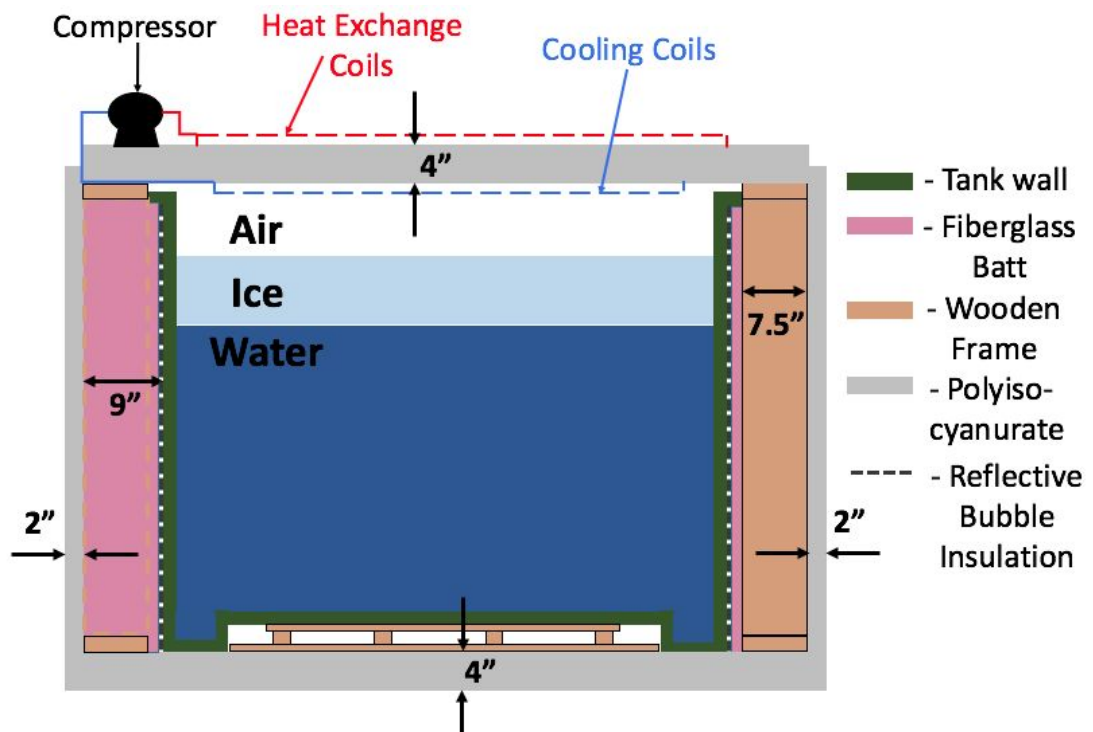


**Figure 22:** The diagram showing the insulation amounts and cooling system setup for the tank design version 3 (final design).



In order to ensure that heat losses through the bottom of the tank were minimized, two 2 inch 4x8 foot polyiso insulation sheets were cut and formed into a 4 inch base for the tank to sit on. A small 4x4 foot frame was built to go underneath the tank to support the base of the tank where bowing occurred in the previous design. A wooden frame was then built on top of this to hold strips



**Figure 24:** Assembly of outer insulation

of the same fiberglass insulation used before. This would allow for a cleaner and tighter fit to the tank walls. After the fiberglass insulation was hung, industrial adhesive was used to attach a layer of 2 inch thick polyiso insulation board to the exterior of the wooden frame with edges overlapping to cut down on losses. A dual layer of 2 inch thick polyiso was used to construct a lid that would sit down within the tank walls and cover the top of the tank. All joints were covered with insulating foil tape to avoid conductive losses through cracks.



**Figure 23:** Final insulated base and frame

The cooling system was also revamped in this version. The previously utilized chest freezer was taken apart and gutted for its interior components. It was believed that it would not be possible to take this system apart without breaking and/or cutting the condenser or evaporator coils, yet with care the system was salvaged intact. This cut down on both cost and time, as the team did not have to order a compressor recharge kit which would have been necessary if any lines were damaged and coolant was lost.



**Figure 26:** Integrated cooling system and lid

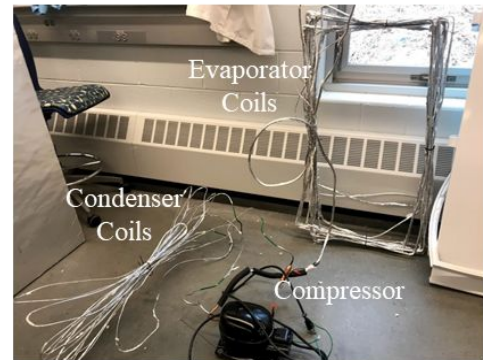


**Figure 25:** Salvaged cooling system

The salvaged cooling system was integrated directly into the new lid of the water tank to allow for ease of removal. This was done by hand bending the condensing coils on the exterior of the lid to allow as much spacing as possible for maximum heat transfer out of the coils, and doing the same with the evaporator

coils on the interior for maximum and even cooling within the tank. The compressor was mounted on the corner of the lid to give the most possible area for the condensing coils on the exterior.

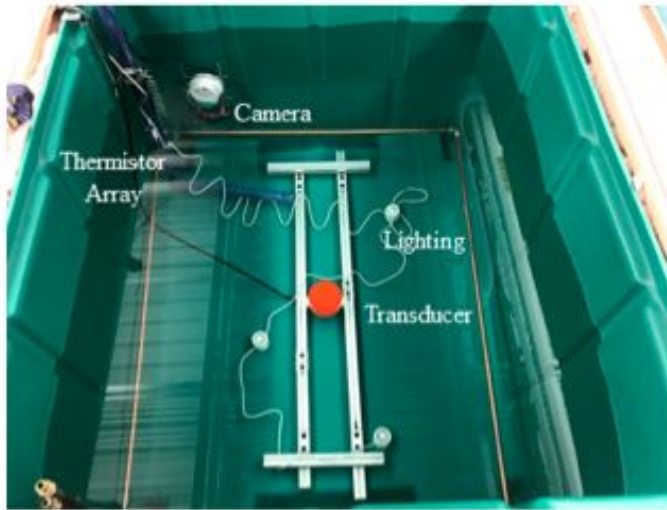


**Figure 27:** Installed Instrumentation within the Final Tank

As a profile of the tank interior was still necessary, the thermistor array was again mounted inside of the water tank. Both above and below water cameras were installed facing a measuring rod with respect to the water line in order to have a visual representation of ice growth. A hand held temperature probe was also placed above the water surface if the tank in order to give a measure of accuracy for the thermistor array. All cables were run out of the tank via a hole in the exterior insulation.

When all of these components were assembled and installed, an industrial chiller was used to cool the initial water temperature down to roughly 9 °C by routing chilled water through copper piping hung within the tank. Once this temperature was reached, the lid to the tank was placed in position and the cooling system was turned on for a trial run.



**Figure 28:** Final Experimental Tank and Instrumentation Setup

### 4.3.2 Trial 2 Results

This current version was left to run for the duration of the experiment and the temperature was constantly monitored via the thermistor array. Over this time period, it was observed that the air temperature in the tank reached below freezing within less than a weeks time span, which was not achieved with the previous iteration of the experiment.

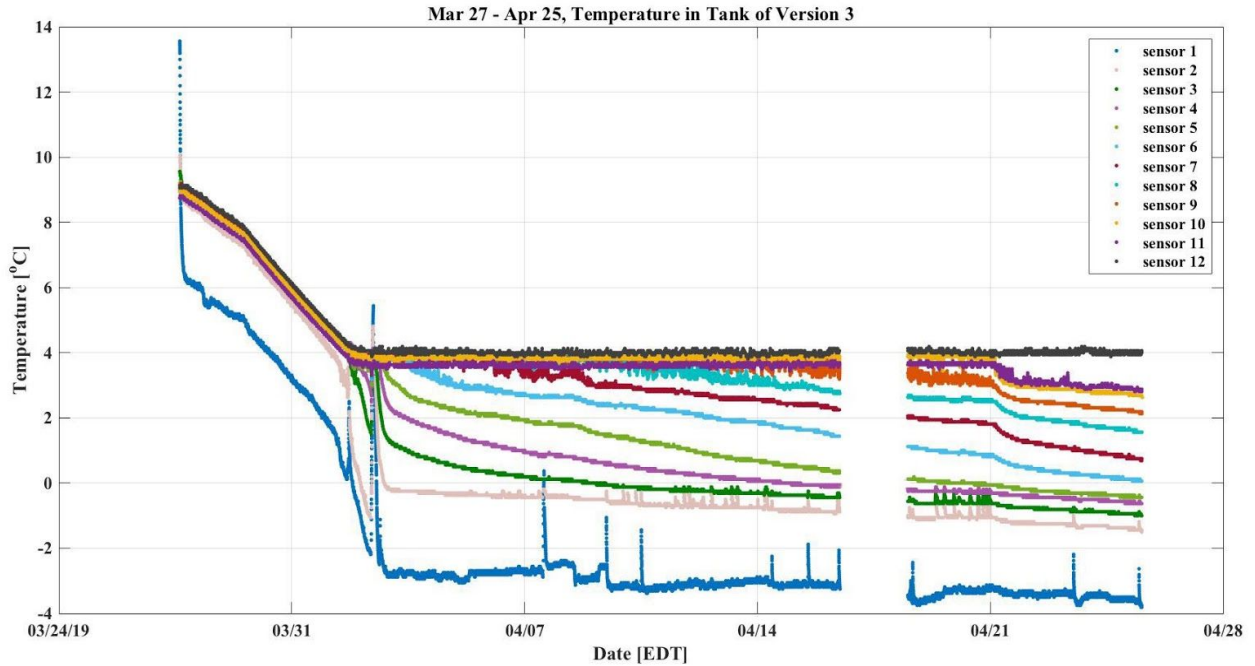


**Figure 29:** The thermistor temperature profile data of the trial test for tank version 3, which started on Mar 27, 2019 and recorded until April 25, 2019.

The vertical peaks in the temperature data since Apr 8 from sensor 1 display the times when the physical ice core samples were collected, due to the top being opened causing the air temperature to drastically increase in a short amount of time. The SD card was not working normally from Apr 16 to Apr 18 so the temperature data was not collected, which caused a gap in the plot. It can be seen that freezing conditions were achieved roughly five days after the beginning of the trial run. Although the temperature did reach below freezing, the system could not achieve anything below  $-3.2\text{ }^{\circ}\text{C}$  due to either the capacity of the cooling system or temperature losses due to insufficient insulation. However, since freezing temperatures were achieved, it was decided that the experiment would continue with this setup. The large temperature spikes seen in the plot above indicate times when the lid was removed to make adjustments, which included defrosting the evaporator coils and adding lines to prevent these coils from sagging.

### 4.3.3 System Analysis

All the instruments were then installed into the tank after the 5-6 day trial run; the cameras capturing time lapse footage, thermistors recording data every minute, and the acoustic transducer pinging every 10 seconds. Then the tank was sealed again, the time of this installation of all the instruments can be seen in both **Figure 29** and **Figure 30** where the spikes in air temperatures occur.



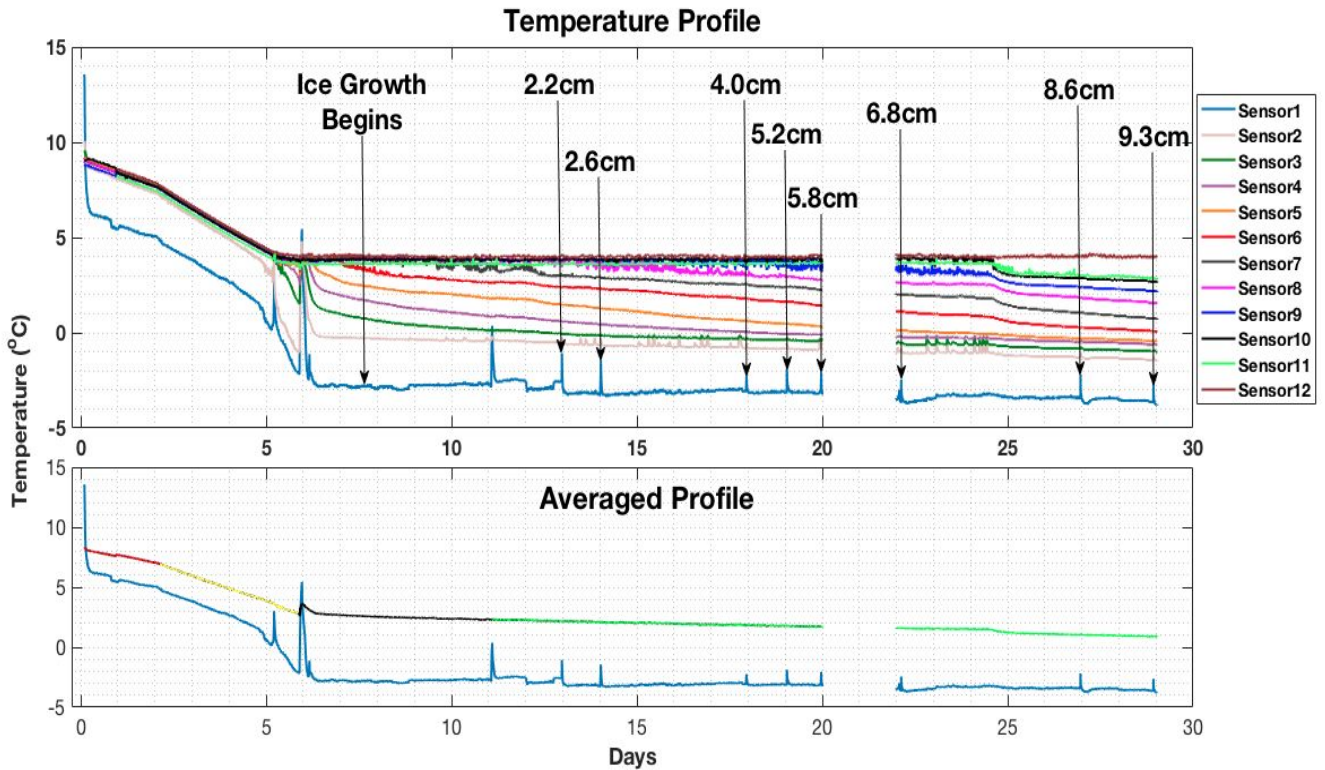


**Figure 30:** Thermistor temperature profile over the duration of the experiment with ice core data callouts on top, and the air temperature and averaged water temperatures on bottom.

Throughout this experiment, the thermistor array continued to collect data, allowing for a calculation of the cooling capacity of the system. It should be noted that the x-axis of time in **Figure 30** above is in days since the start of the trial which correlates with the x-axis of **Figure 32** in the acoustic analysis below. From **Figure 30** the cooling system had approximately three different cooling rates or cooling capacities during the duration of this experiment;

- 64.2 Watts (219 Btu/hr): First 2 days (Red Line)
- 103 Watts (353 Btu/hr): Following 3 days (Yellow Line)
- 11.8 Watts (40.3 Btu/hr): Once ice grew (Green Line)

These cooling capacities were calculated using the rate of change in the averaged water temperature during these different time periods, the mass of water being cooled (calculated with known volume and density), and the specific heat of water ( $c = 4.186 \text{ kJ/kg}^\circ\text{C}$ ). The increase in cooling efficient between the first two days and following 3 days of about 60% can be attributed to the the addition of 3 fans on the top of the tank which blew directly on the condenser coils. This allowed the condenser coils to exchange more heat energy absorbed from within the tank, into the room, vastly improved the efficiency of the cooling system.

Although profiling instrumentation was installed within the tank to monitor this ice growth, the conditions in the tank caused ice to grow almost perfectly clear and without air bubbles, making it almost indistinguishable from the water on the underwater camera feed. This meant that the only accurate way to determine the thickness of the ice would be to take the lid off and perform an ice coring and measurement, which was done every 1 to 3 days after the issue was realized.

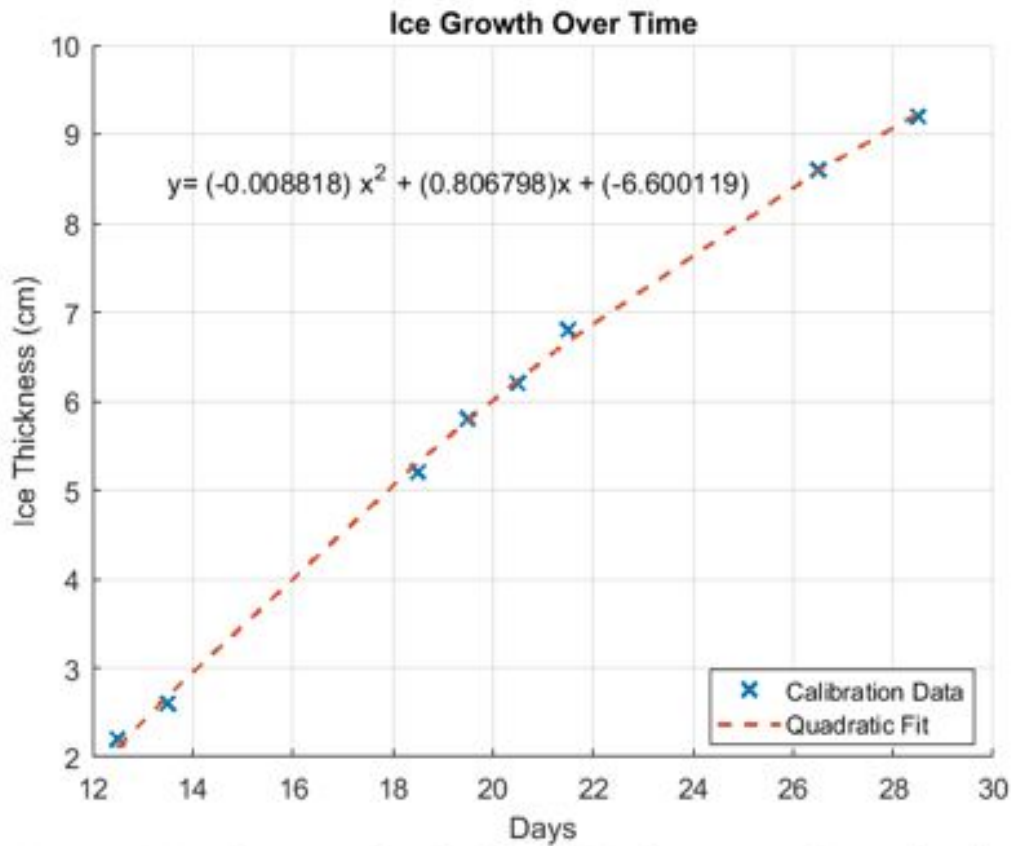


**Figure 31:** The quadratic fit of the ice core data obtained over the duration of the experiment.

The results were plotted against time to achieve a rate of ice growth within the tank. The rate of ice growth within the tank was determined through a quadratic fit of physical ice cores taken within the tank. Doing so yielded an average rate of ice growth of  $0.45 \pm 0.08$  cm per day.

## 5. Acoustic Analysis

Throughout the duration of this experiment, acoustic data was collected on the water-ice and ice-air boundaries. This data was plotted in a time series in order to visualize the changing boundary locations or growing ice thickness. This is shown in **Figure 32** below

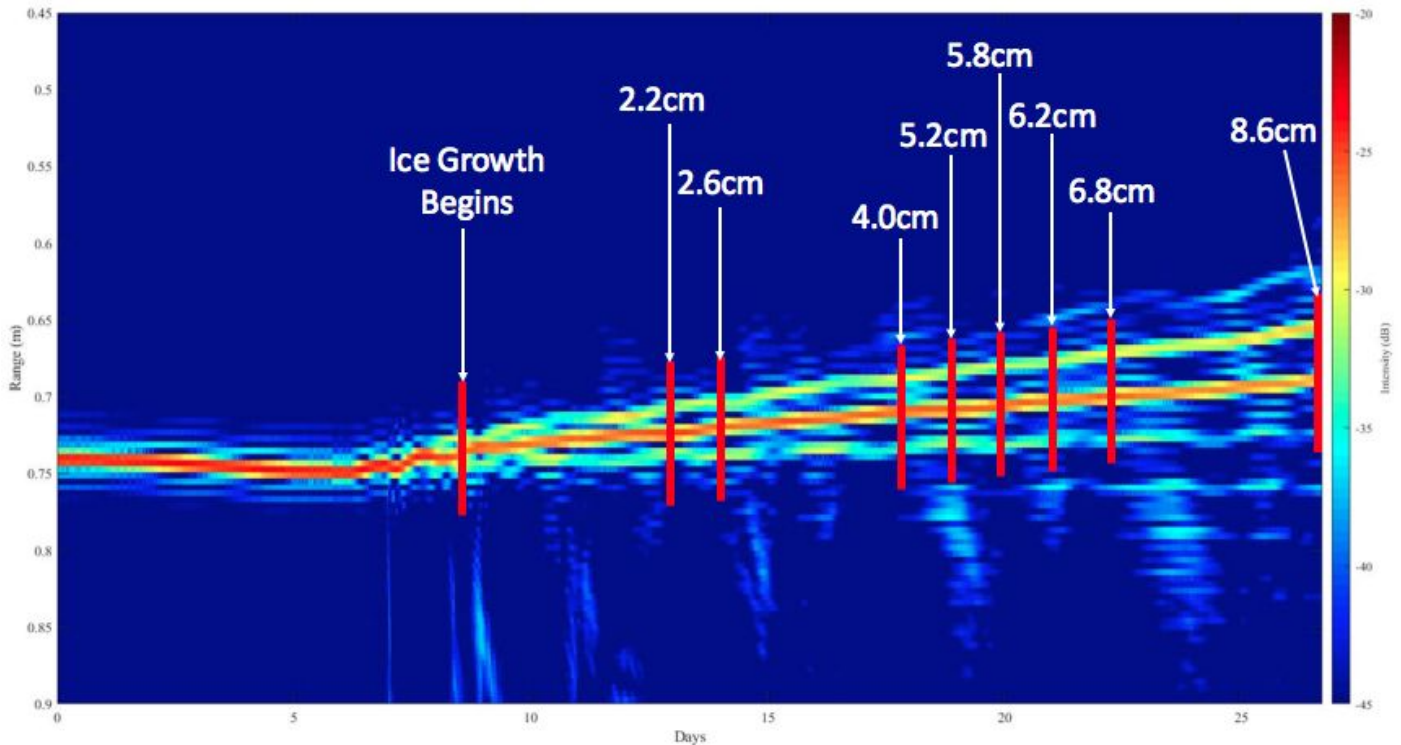


**Figure 32:** Acoustic response of boundary layers throughout course of experiment. Callouts indicate ice core samples

From this image, the change in the distance between boundary layers can easily be seen. For the first seven days of the experiment, the return shows simply water on the surface, which coincides with data obtained from the thermistor array. Beyond this, it can be seen that this reflection's intensity distribution becomes more complicated, and eventually splits into three separate signals. The return closest to the top of the plot indicates the changing water-ice boundary layer and the stronger, middle, signal indicates the location of the ice-air boundary layer. The distance between the strongest return point of these two signals at any given time gives a measure of ice thickness.

It was observed that the first distinguishable separation between these beams occurs 10.5 days from the beginning of the experiment. Using the quadratic fit of ice growth data obtained from core samples, it was determined that at this point 1.15 cm of ice would have grown. Knowing this, it can be stated that a conservative estimate of the resolution of the acoustic measurement is 1.2 centimeters.

A single pulse response from the acoustic data at an ice thickness of 6.8cm was plotted next to the predicted acoustic response at the same ice thickness (6.8cm) in order to compare both the shape and magnitude of the reflected responses.

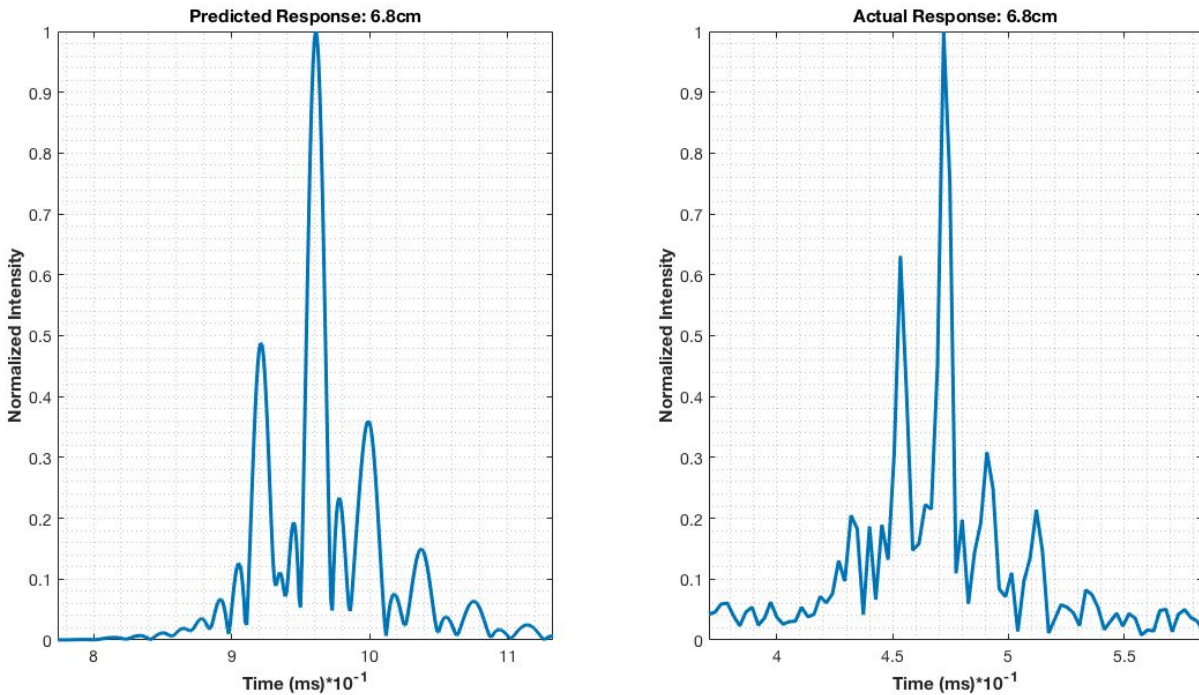


**Figure 33:** A comparison between the predicted received acoustic pulse response (left) and the actual received acoustic pulse response (right) for 6.8cm of ice thickness.

It can be seen that the boundary response shape corresponds with what was predicted by the acoustic model. The response shape validates the acoustic model created for this experiment. However, it can be seen that the magnitudes of these responses are different. Both the time delay between the ice boundaries and the intensity reflected from the bottom of the ice differ from the model, and it is believed to be due to the sound speed and density of ice. Exact density values for ice vary as a function of temperature, air content, and other environmental factors. Due to this, the values used in the model may not have been correct. These values are therefore relatively unknown and require future investigation.

It should also be noted that the “Actual” response assumes only the sound speed in water and does not take into account the changing sound speeds through separate boundaries. This was noted and accounted for in the analysis, yet future post processing methods may wish to account for this.

## 6. Conclusions

Throughout the course of this project, three main conclusions emerged. The first of these was that the team was able to design and construct a tank and cooling system capable of housing all required instrumentation while water was cooled and subsequently frozen. Although the team encountered both design and construction errors/delays, two iterations of this system were tested, and a final version operated with sufficient results. This final version was able to chill and cool a large mass of water and thereby freeze it, resulting in an ice growth rate of  $0.45 \pm 0.08$  cm per day after initial ice growth. This growth was not linear however, instead following a quadratic curve with growth slowing as time progressed. Most likely this was due to the insulating properties of ice slowing the rate of cooling provided to the water surface below. The National Snow and Ice Data Center (NSDIC) validate this trend, noting that “The ice thickness increases at a rate roughly proportional to the square root of the cumulative FDD” (nsdic.org). The FDD referred to in this stand for “Freezing Degree Days”, and the noted method follows a non-linear growth that slows in growth rate the thicker the ice grows.

The second conclusion that was reached was that the project succeeded in the goal to measure ice thickness at a high resolution using upwards looking broadband acoustics. The analysis of the received signal from the water and ice boundaries resulted in a system resolution of 1.2 cm. This results is what was hoped for at the onset of the experiment, in that the measurement had a resolution within the centimeter range. A measurement at this resolution is a marked improvement on previous methods of finding ice thickness. This was a measurement taken under ideal, static, conditions however. Field deployments of this system will have more complex conditions to resolve, yet laboratory tests indicate positive results. Some of these complex conditions include, varying ice density and sound speed through actual sea ice, ice thickness of much greater magnitudes, air pockets and salinity channels within the ice and a snow layer on top of the ice.

Finally, it was found that refinement of the speed of sound in ice is necessary. The magnitudes of the responses from the actual reflected pulse differ from those predicted by the model. It was theorized that this is due to the density of and sound speed through the ice which was utilized in the model. This density used was most likely not the exact density of the ice within the tank, as well as the predicted speed of sound through the ice. Because of this, both the distance between responses and the intensity of the reflected signal responses would have been scaled incorrectly.

## 7. Future Recommendations

Much was accomplished in this project, yet there are improvements that can be made to the system and methodology utilized in this project. In order to assist future endeavors in this study, a list of recommendations is included below;

1. Cooling System Improvements: The system cools fairly slowly, at a rate of roughly 0.5cm per day. Although this allows for more data points over the course of the study, growing large quantities of ice takes significant amounts of time. A higher capacity cooling system is recommended in order to freeze ice more rapidly.
  - a. More powerful cooling allows for ice growth under different temperatures provided that a metering device is included
2. Acoustic Measurements: The transducer in this experiment was set to ping at a 10 second interval. As ice was grows relatively slowly over the course of a day, this interval was much faster than required.
  - a. Due to the amount of pings collected throughout the course of the experiment, there was roughly 10 GB of acoustic data collected. Processing this data was done in MATLAB, and each run of the 10 GB of data required roughly 5 hours in order for the code to read the data files and compile them into the correct figures. Refinement of either the code used or the ping rate would cut down on this processing time
3. Physical Ice Measurements: The underwater camera and measuring rod in this experiment were rendered obsolete as the ice was grown perfectly clear. Due to this, physical ice core measurements were required in order to determine growth rates and resolution. A more convenient method should be adapted in order to prevent removing the tank lid to determine ice thickness
4. Thermistor Array: The spacing of the thermistors on the array should be more uniform to provide more precise profiling, and the amount of thermistors could be increased to gain a more comprehensive profile of the entire tank.
5. Ice Density and Sound Speed: As noted before, these measurements require refinement in both the model and the post processing of acoustic data. This will allow for direct measurements of ice data based solely on acoustic data (e.g. without extrapolation of ice growth from ice core data)
6. Insulation: Additional insulation on all sides of the tank but specifically on the bottom to ensure less heat transfer into the tank, tank efficiency.
7. Instrumentation: Additional sensors may be installed in order to monitor oxygen content, salinity, etc. for future experiments under different parameters.

8. Pressurization: Adding gaskets, fasteners and an apparatus to allow for ice growth under different simulated atmospheric conditions would allow for more useful data to be collected for future implementation in the field.

## 8. References

Bob. "Lake Ice." *Ice Growth*, lakeice.squarespace.com/ice-growth/.

Center for International Earth Science Information Network at Columbia University (CIESIN). *PERCENTAGE OF TOTAL POPULATION LIVING IN COASTAL AREAS* . PERCENTAGE OF TOTAL POPULATION LIVING IN COASTAL AREAS .

"Extreme Weather Gets a Boost from Climate Change." *Environmental Defense Fund*, 2019, [www.edf.org/climate/climate-change-and-extreme-weather](http://www.edf.org/climate/climate-change-and-extreme-weather).

"Frigidaire Upright Freezer Blowing Warm Air." *DoItYourself.com Community Forums*, [www.doityourself.com/forum/electric-large-kitchen-home-appliances/554749-frigidaire-upright-freezer-blowing-warm-air.html](http://www.doityourself.com/forum/electric-large-kitchen-home-appliances/554749-frigidaire-upright-freezer-blowing-warm-air.html).

"How We Measure Sea Ice." *Met Office*, [www.metoffice.gov.uk/research/climate/cryosphere-oceans/sea-ice/measure](http://www.metoffice.gov.uk/research/climate/cryosphere-oceans/sea-ice/measure).

Kinsler, Lawrence E, et al. *Fundamentals of Acoustics*. 4th ed., 1999.

"National Snow and Ice Data Center." *Thermodynamics: Growth | National Snow and Ice Data Center*, [nsidc.org/cryosphere/seaice/processes/thermodynamic\\_growth.html](http://nsidc.org/cryosphere/seaice/processes/thermodynamic_growth.html).

Simrad Technologies. "Simrad ES200-7CD." *Simrad.com*, Sept. 2009, [www.simrad.online/td\\_200/es200\\_7cd/es200\\_7cd\\_ds\\_en\\_a4.pdf](http://www.simrad.online/td_200/es200_7cd/es200_7cd_ds_en_a4.pdf).

Struzik, Ed. "Shipping Plans Grow as Arctic Ice Fades." *Yale E360*, 17 Nov. 2017, [e360.yale.edu/features/cargo\\_shipping\\_in\\_the\\_arctic\\_declining\\_sea\\_ice](http://e360.yale.edu/features/cargo_shipping_in_the_arctic_declining_sea_ice).

"The Quickest Way to Break the Ice Is by Submarine." *The Economist*, The Economist Newspaper, 12 Apr. 2017, [www.economist.com/science-and-technology/2017/04/12/the-quickest-way-to-break-the-ice-is-by-submarine](http://www.economist.com/science-and-technology/2017/04/12/the-quickest-way-to-break-the-ice-is-by-submarine).

"The Refrigeration Cycle Explained in Plain English." *The Refrigeration Cycle Explained in Plain English.*, 2005, [www.air-conditioning-and-refrigeration-guide.com/refrigeration-cycle.html](http://www.air-conditioning-and-refrigeration-guide.com/refrigeration-cycle.html).



“Thermodynamics: Growth | National Snow and Ice Data Center.” *National Snow and Ice Data Center*, [nsidc.org/cryosphere/seaice/processes/thermodynamic\\_growth.html](https://nsidc.org/cryosphere/seaice/processes/thermodynamic_growth.html).

University of Texas Rio Grande. *HEAT TRANSFER EQUATION SHEET*.  
[faculty.utrgv.edu/constantine.tarawneh/Heat%20Transfer/HeatTransferBooklet.pdf](https://faculty.utrgv.edu/constantine.tarawneh/Heat%20Transfer/HeatTransferBooklet.pdf).

US Department of Commerce, and National Oceanic and Atmospheric Administration. “How Does Sea Ice Affect Global Climate?” *NOAA's National Ocean Service*, 1 Nov. 2011, [oceanservice.noaa.gov/facts/sea-ice-climate.html](https://oceanservice.noaa.gov/facts/sea-ice-climate.html).

## **Acknowledgements**

Large scale projects such as this require a team effort to be successful. A special thanks to Professor Tom Weber for his funding and intellectual, contributions and advice throughout the course of the year, alongside Research Professor Anthony Lyons and PhD Student Greg Deemer. Without these individuals this project would not have been such a success. We would also like to acknowledge New Hampshire Sea Grant College Program, a federal-university partnership for funding this project as well.

## 9. Appendices

### 9.1 Arduino Code for Thermistor Array

```
#include <OneWire.h>
#include <DallasTemperature.h>
#include <SPI.h>
#include <SD.h>
#include <Wire.h>
#include "string.h"
#include "RTClib.h"

// The loops for sensors in this code are fixed based on the designed number of sensors
// that are connected to each one wire system.
// The loops for sensors are designed to save the space of the script. So if individual adjustment is
// required for each of sensors, the loops need to be restored to singular command within several
// individual void loops.
// The process of finding the address of each sensor is left out in this code once the address is
// found and the sensors are fixed.

//Define the Real Time Clock
RTC_PCF8523 rtc;
const int chipSelect = 10;
File logfile;
void error(const char *str)
{
  Serial.print("error: ");
  Serial.println(str);
  while(1);
}

// Declare Pin Numbers
#define ONE_WIRE_BUS_1_PIN 2
#define ONE_WIRE_BUS_2_PIN 4

// 2 one-wire systems are used
#define num_sensor 2

OneWire oneWire1(ONE_WIRE_BUS_1_PIN);
OneWire oneWire2(ONE_WIRE_BUS_2_PIN);

DallasTemperature sensors[num_sensor] = { DallasTemperature(&oneWire1) ,
DallasTemperature(&oneWire2) };
```

```

DeviceAddress probe[num_sensor][6] = {

    { //onewire system1
      { 0x28, 0xA3, 0xB6, 0xAB, 0x1B, 0x13, 0x01, 0x99 },
      { 0x28, 0xE6, 0xAA, 0x64, 0x1E, 0x13, 0x01, 0xCC },
      { 0x28, 0x08, 0x81, 0x67, 0x1B, 0x13, 0x01, 0xC3 },
      { 0x28, 0xAA, 0xC5, 0xA0, 0x13, 0x13, 0x02, 0x7F },
      { 0x28, 0xAE, 0xD8, 0xB9, 0x1B, 0x13, 0x01, 0x5F },
      { 0x28, 0xEB, 0xDC, 0x68, 0x1E, 0x13, 0x01, 0x65 }
    },

    { //onewire system2
      { 0x28, 0xAA, 0xA0, 0xA6, 0x13, 0x13, 0x02, 0xB5 },
      { 0x28, 0xAA, 0x1E, 0xA4, 0x13, 0x13, 0x02, 0x5F },
      { 0x28, 0x4F, 0x1B, 0x7C, 0x1B, 0x13, 0x01, 0x95 },
      { 0x28, 0x7F, 0x26, 0xC3, 0x1B, 0x13, 0x01, 0x1B },
      { 0x28, 0x9D, 0x02, 0x79, 0x1B, 0x13, 0x01, 0x31 },
      { 0x28, 0xAA, 0x95, 0x97, 0x13, 0x13, 0x02, 0x24 }
    }
};

void setup()
{
  Serial.begin(9600);
  for(int i = 0; i < num_sensor; i++)
    sensors[i].begin();

  for(int i = 0; i < num_sensor*6; i+=1)
    sensors[i/6].setResolution(probe[i/6][i%6], 12);

  // initialize the SD card
  Serial.print("SD card is working Hahahahaha");
  pinMode(10, OUTPUT);

  // see if the card is present and can be initialized:
  if (!SD.begin(chipSelect)) {
    error("Card failed, or not present");
  }
  Serial.println("card initialized.");

  // create a new file
  char filename[] = "VOLTAGES.CSV";
  for (int i = 0; i < 100; i++) {
    filename[6] = i/10 + '0';
  }
}

```

```

filename[7] = i%10 + '0';
if (! SD.exists(filename)) {
  // only open a new file if it doesn't exist
  logfile = SD.open(filename, FILE_WRITE);
  break;
}
}

if (! logfile) {
  error("Couldn't create file");
}
//set up the rtc
while (!Serial) {
  delay(1);
}

Serial.begin(9600);
if (! rtc.begin()) {
  Serial.println("Couldn't find RTC");
  while (1);
}

if (! rtc.initialized()) {
  Serial.println("RTC is running!");
  rtc.adjust(DateTime(F(__DATE__), F(__TIME__)));
}

}
//end setup

void loop()
{
  DateTime now = rtc.now();

  Serial.print(now.year(), DEC);
  Serial.print('/');
  Serial.print(now.month(), DEC);
  Serial.print('/');
  Serial.print(now.day(), DEC);
  Serial.print(',');
  Serial.print(now.hour(), DEC);
  Serial.print(':');
  Serial.print(now.minute(), DEC);
  Serial.print(':');
  Serial.print(now.second(), DEC);

```

```

Serial.print(',');

logfile.print(now.year(), DEC);
logfile.print(',');
logfile.print(now.month(), DEC);
logfile.print(',');
logfile.print(now.day(), DEC);
logfile.print(',');
logfile.print(now.hour(), DEC);
logfile.print(',');
logfile.print(now.minute(), DEC);
logfile.print(',');
logfile.print(now.second(), DEC);
logfile.print(',');

for(int i = 0; i < num_sensor; i++)
    sensors[i].requestTemperatures();

for(int i = 0; i < num_sensor*6; i++)
{
    char str[80];
    char snum[5];
    itoa(i+1, snum, 10);
    strcpy(str, "Probe ");
    if(i < 10)
        strcat(str, "0");
    strcat(str, snum);
    strcat(str, ": ");

    Serial.print(str);
    logfile.print("");
    printTemperature(probe[i/6][i%6], i/6);
    Serial.println();

}

    logfile.println();
    delay(60000);
    logfile.flush();

} // end main loop

void printTemperature(DeviceAddress deviceAddress, int c)
{

```

```

float tempC = sensors[c].getTempC(deviceAddress);

if (tempC == -127.00)
{
  Serial.print("Error getting temperature");
}
else
{
  Serial.print(tempC);
  Serial.print(',');
  logfile.print(tempC);
  logfile.print(',');
}
}
//THE END

```

## 9.2 Matlab Code for Temperature Profile

```

clear all
clc
A = readtable('VOLTAG59.CSV');
B = readtable('VOLTAG61.CSV');
C = readtable('VOLTAG67.CSV');
D = readtable('VOLTAG69.CSV');
E = readtable('VOLTAG70.CSV');
F = readtable('VOLTAG73.CSV');
G = readtable('VOLTAG76.CSV');
H = readtable('VOLTAG79.CSV');
I = readtable('VOLTAG81.CSV');
J = readtable('VOLTAG83.CSV');
K = readtable('VOLTAG84.CSV');
L = readtable('VOLTAG85.CSV');
M = readtable('VOLTAG87.CSV');
N = readtable('VOLTAG90.CSV');
O = readtable('VOLTAG92.CSV');
P = readtable('VOLTAG93.CSV');
Q = readtable('VOLTAG94.CSV');
R = readtable('VOLTAG96.CSV');
S = readtable('VOLTAG98.CSV');
T = readtable('VOLTAG01.CSV');
U = readtable('VOLTAG02.CSV');

```



```

Data1 = A{:,7:16};
Data2 = B{:,7:18};
Data3 = C{:,7:18};
Data4 = D{:,7:18};
Data5 = [E{:,7:18};F{:,7:18}];
Data6 = G{:,7:18};
Data7 = H{:,7:18};
Data8 = I{:,7:18};
Data9 = J{:,7:18};
Data10 = K{:,7:18};
Data11 = L{:,7:18};
Data12 = M{:,7:18};
Data13 = N{:,7:18};
Data14 = O{:,7:18};
Data15 = P{:,7:18};
Data16 = Q{:,7:18};
Data17 = R{:,7:18};
Data18 = S{:,7:18};
Data20 = T{:,7:18};
Data21 = U{:,7:18};
[n1,m1] = size(Data1);
[n2,m2] = size(Data2);
[n3,m3] = size(Data20);
Data1_1 = zeros(n1,m2);
Data1_1(:,1:3) = Data1(:,1:3);
Data1_1(:,5) = Data1(:,4);
Data1_1(:,7:12) = Data1(:,5:10);
Data19 = zeros(2853,12);
Data = [Data1_1;Data2;Data3;Data4;Data5;Data6;Data7;Data8;Data9;Data10;Data11;...
Data12;Data13;Data14;Data15;Data16;Data17;Data18;Data19;Data20;Data21];
[n,m] = size(Data);

t1={'27-Mar-2019 15:13:24'};
t2={'25-Apr-2019 13:48:24'};
t11=datevec(datenum(t1));
t22=datevec(datenum(t2));
time_interval_in_seconds = etime(t22,t11);
del = time_interval_in_seconds/n;

```

```

dates = datenum('Mar 27, 2019 3:13:24 PM'):del/(24*60*60):datenum('Apr 25, 2019 01:48:24
PM');

dates = dates(2:end);
dates_2 = dates(1202:end);

plot(dates,Data(:,1),'.','linewidth',2.5)
hold on
plot(dates,Data(:,2),'.','linewidth',2.5,'color',[0.88 0.75 0.73])
plot(dates,Data(:,3),'.','linewidth',2.5,'color',[0.00 0.50 0.00])
plot(dates_2,Data(1202:end,4),'.','linewidth',2.5,'color',[0.66 0.34 0.65])
plot(dates,Data(:,5),'.','linewidth',2.5)
plot(dates_2,Data(1202:end,6),'.','linewidth',2.5)
plot(dates,Data(:,7),'.','linewidth',2.5)
plot(dates,Data(:,8),'.','linewidth',2.5,'color',[0 0.75 0.75])
plot(dates,Data(:,9),'.','linewidth',2.5)
plot(dates,Data(:,10),'.','linewidth',2.5)
plot(dates,Data(:,11),'.','linewidth',2.5)
plot(dates,Data(:,12),'.','linewidth',2.5,'color',[0.25 0.25 0.25])
dynamicDateTicks
grid on
xlabel('Date [EDT]')
ylabel('Temperature [°C]')
legend('sensor 1','sensor 2','sensor 3','sensor 4','sensor 5','sensor 6',...
'sensor 7','sensor 8','sensor 9','sensor 10','sensor 11','sensor 12')
title('Mar 27 - Apr 25, Temperature in Tank of Version 3')
set(gca,'PlotBoxAspectRatio',[2 1 1])
set(gca,'fontweight','bold');
set(gca,'fontsize',12);
set(gca,'fontname','Times New Roman');

```

### 9.3 Matlab Code for Far-Field and Beam Pattern Model

```
clear all; close all; clc
```

```

f = 200000; % frequency of piston transducer (Hz)
po = 1000; % density of water (kg/m^3)
c = 1403; % sound speed in water (m/s)

```

```

Uo = 1; % uniform normal source velocity, magnitude doesnt matter since it occurs in both
equations
k = (2*pi*f)/c; % wave number (radians/m)
a = .0295; % radius of piston transducer (m)
ka = k*a;

r = 0:.001:1; % range that pressures are being calculated over

Pax = 2*po*c*Uo.*abs( sin( 0.5.*k.*r.*(sqrt(1+(a./r).^2)-1) ) ); % Axial Piston transducer
Pressure equation (7.4.5)
Pasm = 0.5*po*c*Uo.*(a./r)*ka; % Asymptotic far field axial Piston transducer Pressure
equation (7.4.7)

TenPercentDiff = Pasm - 0.03*Pasm; % 5% difference from Asymptotic solution

for i = 1:length(r)
    if Pax(i)>=TenPercentDiff(i) % finding when the axial piston pressure is within 10% of
asymptotic solution
        RFF(i) = r(i);
    end
end

IndRFF = find(RFF > 0,1,'first');

Ro = r(IndRFF) % range at which farfield is reached

% Near-field / Far - field
figure(1)
plot(r,Pax,'linewidth',3)
hold on
plot(r,Pasm,'r','linewidth',3)
y1 = get(gca, 'ylim');
plot([Ro Ro], y1,'k','linewidth',2)
ylim([0 0.5e7])
grid minor
xlabel('Range (m)','fontsize',18)
ylabel('Pressure Amplitude (Pa)','fontsize',18)
ab = get(gca,'XTickLabel');
set(gca,'XTickLabel',ab,'fontsize',16)
legend('Axial Piston Pressure Amplitude','Asymptotic Form of Axial Piston Pressure
Amplitude','Far-Field Used for Sizing','fontsize',16)
title('Near/Far-Field Model: Simrad ES200-7CD','fontsize',20,'FontWeight','bold')
%% Beam Pattern
theta = -90:0.01:90; % range of steering angles

```

```

v = ka.*sind(theta); % this and H below were obtained from equation 7.4.18 in the book
H = abs((2.*besselj(1,v))./v); % first order besselj is used in the directional factor equation for a
piston
BP = 20.*log10(H); % beam pattern 7.6.1

dB = -3; % beam width cut off dB

IndBeamWidth = find(BP>=dB);
IndBW1 = IndBeamWidth(1);
IndBW2 = IndBeamWidth(end);

ThreedB(1: IndBW2 - IndBW1 +1) = dB;

figure(2)
plot(theta(IndBW1:IndBW2), ThreedB,'r','linewidth',2)
hold on;
plot(theta,BP,'linewidth',3)
ylim([-50 0])
xlim([-90 90])
grid minor
title('Beam Pattern','fontsize',18)
xlabel('Transmit Angle (Degrees)','fontsize',18)
ylabel('Intensity (dB)','fontsize',24)
legend('3dB Beamwidth = 7 Degrees','location','best','fontsize',18)
ab = get(gca,'XTickLabel');
set(gca,'XTickLabel',ab,'fontsize',16)

BeamWidth = theta(IndBW2) - theta(IndBW1)

```

## 9.4 Matlab Code for the Initial and Reflected Pulse Response

```

clear all; close all; clc

%% Pulse Model (in time domain)
fo = 160e3; % 160kHz
ff = 260e3; % 260 kHz
T = 0.512e-3; % pulse length .512 ms in seconds
m = (ff - fo)/(2*T); % linear modulation coefficient

delta_t = 1/1e6; % time step
t1 = [0:delta_t:T]; % time array from 0s to T
t2 = [T+delta_t:delta_t:5*2/1500]; % time from the end of the pulse to 5m distance
t = [t1 t2];

% the actual transmitted signal uses a tukey window as follows, and using this helps interpret the

```

```
% result (the window gets rid of some sidelobes in the response that are difficult to distinguish
% from the reflections
```

```
A = tukeywin(length(t1),.2);
```

```
s = A.*exp(j*2*pi.*(fo + m.*t1).*t1); % pulse that occurs from 0 to .512 milliseconds
```

```
st = [zeros(1,length(t2)/2) s zeros(1,length(t2)/2)]; % padding with zeros to a distance of 5m
```

```
% subplot(2,2,1)
% plot(t,real(st))
% ylim([-1.5 1.5])
% xlabel('Time (ms)','fontsize',25)
% ylabel('Amplitude','fontsize',25)
% grid minor
% xlim([t(1) t(end)])
% title('s(t): LFM Pulse','fontsize',28)
% a = get(gca,'XTickLabel');
% set(gca,'XTickLabel',a,'fontsize',20,'FontWeight','bold')
```

```
figure(1)
plot(t, real(st))
ylim([-1.5 1.5])
xlabel('Time (ms)','fontsize',18)
ylabel('Pressure Amplitude (Pa)','fontsize',18)
xlim([t(3000) t(end-3000)])
grid minor
title('LFM Pulse Model','fontsize',20)
%title('Zoomed In','fontsize',28,'FontWeight','bold')
a = get(gca,'XTickLabel');
set(gca,'XTickLabel',a,'fontsize',16)
```

```
% Pulse Model (in frequency domain)
Sf = fft(st); % Fourier transform of the padded pulse signal
```

```
% Make the frequency vector:
T = delta_t*length(st);
df = 1/T;
fs = 1/delta_t;
freq = 0:df:(fs-df);
```

```
figure(2)
plot(freq, abs(Sf),'linewidth',3)
grid minor
title('Frequency Distribution of The Modeled Pulse','fontsize',20)
xlabel('Frequency (Hz)*10^5','fontsize',18)
```

```

ylabel('Spectral Density','fontsize',18)
xlim([freq(1) freq(end-3700)])
a = get(gca,'XTickLabel');
set(gca,'XTickLabel',a,'fontsize',16)

%% Reflection Coefficient Predictions through various ice thicknesses
%D = [0:0.005:.2]; % 20cm thickness with 5mm stepsize
D = [0:.01:.1];

rho_w = 1000; % density of water; kg/m^3
rho_i = 917; % density of Ice (0 C): kg/m^3
rho_a = 1.225; % density of Air: kg/m^3

c_w = 1490; % sound speed in water: m/s
c_i = 3500; % sound speed in ice: m/s
c_a = 343; % sound speed in air (at room temp): m/s

kw = (2*pi*freq)/c_w; % wave number for water layer
ki = (2*pi*freq)/c_i; % wave number for ice layer
ka = (2*pi*freq)/c_a; % wave number for air layer

R = zeros(length(D),length(freq));

for n = 1:length(D)
    for i = 1:length(freq)
        A = [ 1, -1, -1, 0; -1, -(rho_w*c_w)/(rho_i*c_i), (rho_w*c_w)/(rho_i*c_i), 0;...
            0, exp(-j*ki(i)*D(n)), exp(j*ki(i)*D(n)), -exp(-j*ka(i)*D(n));...
            0, exp(-j*ki(i)*D(n)), -exp(j*ki(i)*D(n)), -((rho_i*c_i)/(rho_a*c_a))*exp(-j*ka(i)*D(n))];

        B = [-1; -1; 0; 0];

        C(i,1:4) = (A\B); % solution to the matrix problem columns go [R, A, B, T]
        Rvec = C(:,1)';
    end
    R(n,:) = Rvec;
    SR(n,:) = ifft(Sf.*R(n,:));
end

%% Matched Filter: Reflected Pulse Prediction

% figure(3)
% plot(t, SR(1,:)) %% this is the raw received waveform from the ice

%this is one way to do the match filter - simply a replica correlator
% NORMALIZE THIS

```

```

for i = 1:length(D)
    mf_output1(i,:) = xcorr(s,SR(i,:));
    Max(i) = max(abs(mf_output1(i,:)));
    mf_output(i,:) = abs(mf_output1(i,:))./Max(i);
    %mf_output1(i,:) = conv(fliplr(conj(s)),SR(i,:));
end

% add Time for x value
figure(3)
plot(t, abs(mf_output(7,1:length(t))), 'Color',[0 0.5 .7], 'linewidth',6)
xlim([t(3450) t(end-2850)])
grid minor
xlabel('Time (ms)', 'fontsize',40, 'FontWeight', 'bold')
ylabel('Normalized Intensity', 'fontsize',40, 'FontWeight', 'bold')
title('Reflected Pulse Response: 5cm Ice', 'fontsize',44, 'FontWeight', 'bold')
a = get(gca, 'XTickLabel');
set(gca, 'XTickLabel', a, 'fontsize',26)

```

## 9.5 Matlab code for Cooling Capacity of the System

```

clear all; close all;clc

Data1 = csvread('VOLTAG59.CSV');
Data2 = csvread('VOLTAG61.CSV');
Data3 = csvread('VOLTAG67.CSV');
Data4 = csvread('VOLTAG69.CSV');
Data5 = csvread('VOLTAG70.CSV');
Data6 = csvread('VOLTAG73.CSV');
Data7 = csvread('VOLTAG76.CSV');
Data8 = csvread('VOLTAG79.CSV');
Data9 = csvread('VOLTAG81.CSV');
Data10 = csvread('VOLTAG83.CSV');
Data11 = csvread('VOLTAG84.CSV');
Data12 = csvread('VOLTAG85.CSV');
Data13 = csvread('VOLTAG87.CSV');
Data14 = csvread('VOLTAG90.CSV');
Data15 = csvread('VOLTAG92.CSV');
Data16 = csvread('VOLTAG93.CSV');
Data17 = csvread('VOLTAG94.CSV');
Data18 = csvread('VOLTAG96.CSV');
Data19 = csvread('VOLTAG98.CSV');

Data2 = Data2(:,1:18);
Data6 = Data6(:,1:18);
Data8 = Data8(:,1:18);

```



```

Data9 = Data9(:,1:18);
Data11 = Data11(:,1:18);
Data12 = Data12(:,1:18);
Data13 = Data13(:,1:18);
Data14 = Data14(:,1:18);
Data15 = Data15(:,1:18);
Data16 = Data16(:,1:18);
%%
Data = [Data2;Data3;Data4;Data5;Data6;Data7;Data8;Data9;Data10;Data11;Data12;...
        Data13;Data14;Data15;Data16;Data17;Data18;Data19];

MatTime2 = datenum(Data(:,1), Data(:,2), Data(:,3), Data(:,4), Data(:,5), Data(:,6));
FirstInterval = datenum(Data1(:,1),Data1(:,2),Data1(:,3),Data1(:,4),Data1(:,5),Data1(:,6));
MatTime1 = [FirstInterval;MatTime2];

Sensor1 = [Data1(:,7);Data(:,7)];
Sensor2 = [Data1(:,8);Data(:,8)];
Sensor3 = [Data1(:,9);Data(:,9)];
Sensor4 = [Data1(:,10);Data(:,10)];
Sensor5 = [Data1(:,11);Data(1:5928,11);4;4;Data(5931:end,11)];
Sensor6 = [Data1(:,12);Data(:,12)];
Sensor7 = [Data1(:,13);Data(:,13)];
Sensor8 = [Data1(:,14);Data(:,14)];
Sensor9 = [Data1(:,15);Data(:,15)];
Sensor10 = [Data1(:,16);Data(:,16)];
Sensor11 = Data(:,17);

Fix12(1:22,1) = 4.19;
Sensor12 = [Data(1:5928,18);Fix12;Data(5951:12595,18);Data(12596:end,18)];
for i = 1:length(Sensor12)
    if Sensor12(i) == 0
        Sensor12(i) = 4;
    end
end

Sensor1_2 = Data(:,7);
Sensor2_2 = Data(:,8);
Sensor3_2 = Data(:,9);
Sensor4_2 = Data(:,10);
Sensor5_2 = [Data(1:5928,11);4;4;Data(5931:end,11)];
Sensor6_2 = Data(:,12);
Sensor7_2 = Data(:,13);
Sensor8_2 = Data(:,14);
Sensor9_2 = Data(:,15);
Sensor10_2 = Data(:,16);

```

```

%%
% Zeroing time/matching it with Transducer time
TansducerStart = datenum(2019,03,27,12,57,36);
Time_Zeroed = MatTime1 - TansducerStart;

figure(1)
subplot(5,1,1:3)
plot(Time_Zeroed, Sensor1,'linewidth',2)
hold on
plot(Time_Zeroed, Sensor2,'linewidth',2)
plot(Time_Zeroed, Sensor3,'linewidth',2)
plot(Time_Zeroed, Sensor4,'linewidth',2)
plot(Time_Zeroed, Sensor5,'linewidth',2)
plot(Time_Zeroed, Sensor6,'linewidth',2)
plot(Time_Zeroed, Sensor7,'linewidth',2)
plot(Time_Zeroed, Sensor8,'linewidth',2)
plot(Time_Zeroed, Sensor9,'linewidth',2)
plot(Time_Zeroed, Sensor10,'linewidth',2)
plot(Time_Zeroed(1202:end), Sensor11,'linewidth',2)
plot(Time_Zeroed(1202:end), Sensor12,'linewidth',2)
grid minor
legend('Sensor1','Sensor2','Sensor3','Sensor4','Sensor5','Sensor6','Sensor7','Sensor8',...
'Sensor9','Sensor10','Sensor11','Sensor12','location','west')
a = get(gca,'XTickLabel');
set(gca,'XTickLabel',a,'fontsize',20)
xlabel('Days','fontsize',30,'FontWeight','bold')
ylabel('Temperature (C)','fontsize',30,'FontWeight','bold')
title('Temperature Profile','fontsize',40,'FontWeight','bold')
xlim([-0.25 20.25])

% Average water temp excluding sensors 11 and 12 which didnt have data from
% 3/27 @ 15:13 to 3/28 @ 11:49
WaterTempAVG_1 = (Sensor2(1:1201)+Sensor3(1:1201)+Sensor4(1:1201)+Sensor5(1:1201)...
+Sensor6(1:1201)+Sensor7(1:1201)+Sensor8(1:1201)+Sensor9(1:1201)+Sensor10(1:1201))/10;

% Average water temp of all sensors from 3/28 @ 11:55 to 4/1 @ 16:57
WaterTempAVG_2 = (Sensor2_2+Sensor3_2+Sensor4_2+Sensor5_2+Sensor6_2+Sensor7_2...
+Sensor8_2+Sensor9_2+Sensor10_2+Sensor11+Sensor12)/12;

WaterTempAVG_8in_Ice_Water =
(Sensor2+Sensor3+Sensor4+Sensor5+Sensor6+Sensor7+Sensor8+Sensor9)/8;

AverageWaterTemp = [WaterTempAVG_1;WaterTempAVG_2];

```

```

AVG_Slope1 = AverageWaterTemp(1:2830);
AVG_Slope2 = AverageWaterTemp(2831:8000);
AVG_Slope3 = AverageWaterTemp(15350:end);

AVG_Slope4 = WaterTempAVG_8in_Ice_Water(15350:end);

subplot(5,1,4:5)
plot(Time_Zeroed, Sensor1,'linewidth',2)
hold on
plot(Time_Zeroed, AverageWaterTemp,'k','linewidth',2)
plot(Time_Zeroed(1:2830),AVG_Slope1,'r','linewidth',2)
plot(Time_Zeroed(2831:8000),AVG_Slope2,'y','linewidth',2)
plot(Time_Zeroed(15350:end),AVG_Slope3,'g','linewidth',2)
%plot(Time_Zeroed(8700:end),AVG_Slope3,'m','linewidth',2)
a = get(gca,'XTickLabel');
set(gca,'XTickLabel',a,'fontsize',20)
title('Averaged Profile','fontsize',30,'FontWeight','bold')
grid minor
xlabel('Days','fontsize',30,'FontWeight','bold')
%legend('Air Temp','Average Temp Through all Layers','location','best')
%ylabel('Temperature (C)','fontsize',40,'FontWeight','bold')
%xlabel('Days','fontsize',40,'FontWeight','bold')

Slope1 = mean(diff(AVG_Slope1))/mean(diff(Time_Zeroed(1:2830)))
Slope2 = mean(diff(AVG_Slope2))/mean(diff(Time_Zeroed(2830:7060)))
Slope3 = mean(diff(AVG_Slope3))/mean(diff(Time_Zeroed(8700:end)))

Slope4 = mean(diff(AVG_Slope4))/mean(diff(Time_Zeroed(8700:end))) % First ~4 inches of
water underneath ice

Duration1 = MatTime1(2830) - MatTime1(1)
Duration2 = MatTime1(7060) - MatTime1(2830)
Duration3 = MatTime1(end) - MatTime1(8700)

Mw = 2000; % was of water in kg
c = 4.186; % kj/(kg*K)
dT = -1;

kJperDeg = Mw*c*dT; % amount of heat energy needed to cool water by 1 degree

BtuperDeg = 0.947817*kJperDeg;
BtuperHour1 = Slope1*BtuperDeg/24
BtuperHour2 = Slope2*BtuperDeg/24
BtuperHour3 = Slope3*BtuperDeg/24
BtuperHour4 = Slope4*BtuperDeg/24

```